AIMS Mathematics, 8(12): 30731–30759.
DOI: 10.3934/math.20231571
Received: 03 August 2023
Revised: 17 October 2023
Accepted: 27 October 2023
Published: 14 November 2023

http://www.aimspress.com/journal/Math

Research article

Enhanced evolutionary approach for solving fractional difference recurrent neural network systems: A comprehensive review and state of the art in view of time-scale analysis

Hanan S. Gafel[1] **and Saima Rashid**[2,3,*]

[1] Department of Mathematics and Statistics, College of Science, Taif University, P.O. Box 11099, Taif 21944, Saudi Arabia

[2] Department of Mathematics, Government College University, Faisalabad 38000, Pakistan

[3] Department of Natural Sciences, School of Arts and Sciences, Lebanese American University, Beirut 11022801, Lebanon

* **Correspondence:** Email: saimarashid@gcuf.edu.pk.

Abstract: The present research deals with a novel three-dimensional fractional difference neural network model within undamped oscillations. Both the frequency and the amplitude of movements in equilibrium are subsequently estimated mathematically for such structures. According to the stability assessment, the thresholds of the fractional order were determined where bifurcations happen, and an assortment of fluctuations bifurcate within an insignificant equilibrium state. For such discrete fractional-order connections, the parameterized spectrum of undamped resonances is also predicted, and the periodicity and strength of variations are calculated computationally and numerically. Several qualitative techniques, including the Lyapunov exponent, phase depictions, bifurcation illustrations, the $0-1$ analysis and the approximate entropy technique, have been presented with the rigorous analysis. These outcomes indicate that the suggested discrete fractional neural network model has crucial as well as complicated dynamic features that have been affected by the model's variability, both in commensurate and incommensurate cases. Furthermore, the approximation entropy verification and $\mathbb{C}_0$ procedure are used to assess variability and confirm the emergence of chaos. Ultimately, irregular controllers for preserving and synchronizing the suggested framework are highlighted.

Keywords: discrete fractional difference equations; undamped oscillations; bifurcation; chaos control; master and slave system; time scale
Mathematics Subject Classification: 46S40, 47H10, 54H25

1. Introduction

Numerous scholars in a broad spectrum of scientific and technological disciplines have studied chaotic, evolving networks. Despite the fact that chaos first became identified and researched in continuous-time mechanisms, its prevalence and distinctive features in discrete-time applications additionally piqued the attention of researchers. The logistic map [1], the Tent map [2], Arnold's cat map [3], the beta chaotic map [4], the double rotor map [5] and the Bogdanov map [6] have all been studied throughout several decades.

In recent times, fractional calculus (FC) has been recognized for possessing exceptional features compared to traditional calculus in modeling the fluctuation of occurrences in nature [7]. The advancements in FC are limitless. As illustrations, consider technology [8], biological sciences [9] and epidemics [10]. Despite the fact that continuous-time FC has been around approximately for generations, novel varieties of fractional operators have been continually established [11–14]. An understanding of the intricate functioning of fractional-order (FO) mechanisms is gaining prominence as a major issue in many multidisciplinary areas. The research conducted has noticed that FO systems, including classical-order frameworks, exhibit limit cycles. In particular, Ahmad et al. [15] demonstrated that limit periods are capable of being accomplished in the FO Wien-bridge oscillator, and [16] demonstrated the presence of restricted phases in the fractional Brusselator. Cao et al. [17] investigated the chaotic behavior of a fractional rub-impact turbine structure, while El-Saka et al. [18] provided a computer simulation of a Hopf-type splitting in a FO structure.

Hopfield [19] proposed an improved neural network (NN) structure in 1984, whereby all circuitry is depicted via a straightforward network composed of resistance and a voltage-controlled capacitor and is linked to the adjacent neural pathways via unpredictable sinusoidal stimulation operations. Since that time, evolving aspects of many kinds of NN algorithms have emerged as the focus of significant studies [20–22]. These activities in NN scenarios, nevertheless, lack consideration of FO differences. Several scientists and practitioners are currently attempting to simulate real-world interpretations employing FO difference formulations. In biological processes, it was eventually determined that the cellular filters that constitute biological tissue have FO conductivity [23] and consequently qualify as FO mechanisms. Furthermore, it was subsequently demonstrated that FO frameworks outperform classical-order algorithms when demonstrating the activity of cerebral vestibule-oculomotor NNs [24].

Fractional mechanisms are presently identified in the context of chaos to exhibit broadened interactions in regards to the intensity of chaotic behavior, such as maximum Lyapunov exponents (MLEs), as well aa a variety of drawbacks [25, 26]. The result has prompted plenty of scientists to focus on developing a system for discrete FC (DFC), a previously yet-to-be-discovered field. There are two of the most important investigations in the discipline [27]. At the moment, only a handful of these above-mentioned typical discrete-time mechanisms have been developed and expanded to the fractional difference situation [28]. We recognize that while several fractional illustrations have been floated within the research, they have not yet been put forth in their difference structures [29, 30].

In the present paper, we are particularly interested in persistent NNs. We aim to broaden this representation to the discrete fractional-order (DFO) scenario and examine the consequent technique's interactions. To determine the differences among the asynchronously steady and chaotic categories, we investigate bifurcation visualizations while offering challenging exploratory restrictions on the DFO. These suggested fractional methods associated with these illustrations have been determined to exhibit

potential interactions. In addition to phase diagrams and bifurcation schematics, we verify the presence of chaos in these representations using a theoretical estimation of the MLE. This is accomplished through the implementation of a fractional Jacobian approach to expansion.

However, the fundamental inspiration for this investigation is to evaluate the advantages of DFO recurrent NNs involving undamped oscillations. The limited research on fractional diagrams of chaos in the scientific community appears to concur that fractional difference includes damping degrees of freedom in the combination. Apart from being immensely susceptible to slight modifications in the settings and initial conditions (ICs), the mechanism's pathways additionally become responsive to fluctuations in the DFO [31]. As a result, some argue that fractional illustrations have advantages for processes that include confidential information and signal processing. Other characteristics of fractional visualizations encompass more straightforward shapes and more evolving interactions [32]. Edelman [33] presented the stabilization of equilibria and chaos in FO frameworks as the process whereby convergence arises. The result describes more elaborate patterns of speculation. Consequently, the investigation of the chaotic dynamics of NN models based on commensurate and noncommensurate fractional differences as well as their synchronization and control, is an attractive subject.

Inspired by the consolidation of the cyclic connections of the neurons, the stabilization of unstable environments is frequently and widely researched in the scientific literature [34, 35]. It is the adaptable management of a chaotic mechanism that forces all levels to diminish as time elapses. To the best of our comprehension, no research of this kind for DFO diagrams has been found, which inspired our inquiry. There is no comprehensive bifurcation descriptive hypothesis formulated for the context of DFO evolving mechanisms, so the bifurcation hypothesis in DFO unpredictable platforms remains a pending issue. A further crucial component of chaotic mechanisms is synchronization, which is the procedure of forcing a slave framework to adhere to the same pattern as a master using adaptable influence factors. There are many research papers in the field on the synchronization of classical chaotic and hyper-chaotic structures [36, 37], with just a handful on FO mechanisms [38, 39].

Adopting the above proclivity, we intend in this paper to explore and study the dynamic behaviors of the new (DFNN) model with undamped oscillations using commensurate as well as incommensurate orders. The basic properties of this fractional model will be studied using certain theoretical and numerical analyses. Furthermore, we will use the approximate entropy test and $\mathbb{C}_0$ algorithm to measure the complexity and validate the presence of chaos in the proposed system. In addition, we propose nonlinear controllers that enable stabilizing and synchronizing the suggested model by forcing the states to converge toward zero asymptotically. Additionally, we suggested an ensemble synchronization initiative based on the suggested DFO visualizations, in which the master is concurrently synchronized to an amalgamation of a pair of slave networks. Finally, we will conclude the study by summarizing the most significant findings obtained in the article.

Since DFC is novel, and the associated terminologies are still evolving, Section 2 will offer certain essential accompaniments and equilibrium hypotheses. Section 3 addresses the equilibrium, bifurcations, and undamped fluctuations of DFO recurrent NNs, as well as their bifurcation diagrams and exploratory limitations on DFO that ensure chaotic behavior. Initially, for the commensurate order DFNN, the robustness realm of the insignificant state of equilibrium has been entirely characterized. Taking into consideration the stability analysis, we find the threshold of DFO values at which discontinuities develop and an assortment of resonances split from the superficial equilibrium state.

Notably, the incommensurate order DFNN may demonstrate a bifurcation when an association factor experiences an essential threshold that must be precisely identified. It is important to highlight that the findings in this work can be used to create neurological fluctuations with a specified regularity and intensity by modifying the DFO network configurations. In Section 4, we implement the $0-1$ procedure, the approximate entropy (ApEn) examination, and the $\mathbb{C}_0$ technique to assess challenges and demonstrate the presence of chaos throughout the identified framework. Also, we provide responsive regulators to regulate and synchronize the chaotic pathways of the proposed discrete fractional neural network (DFNN) model. Ultimately, Section 6 presents the overall paper's final analysis.

2. Model configuration of the DFNN

Ruiz et al. [40] implemented a particular category of **n**-node persistent NNs wherein we can acquire and simulate self-sufficiently a special group of dynamic recurring indications, as illustrated in Figure 1. Each neuron receives a multiplied version of inputs and random weights, which is then added with a static bias value (unique to each neuron layer); this is then passed to an appropriate activation function, which decides the final value to be given out of the neuron. There are various activation functions available as per the nature of the input values. Once the output is generated from the final neural net layer, the loss function (input vs. output) is calculated, and back propagation is performed, where the weights are adjusted to make the loss minimum. Finding optimal values of weights is what the overall operation focuses on.

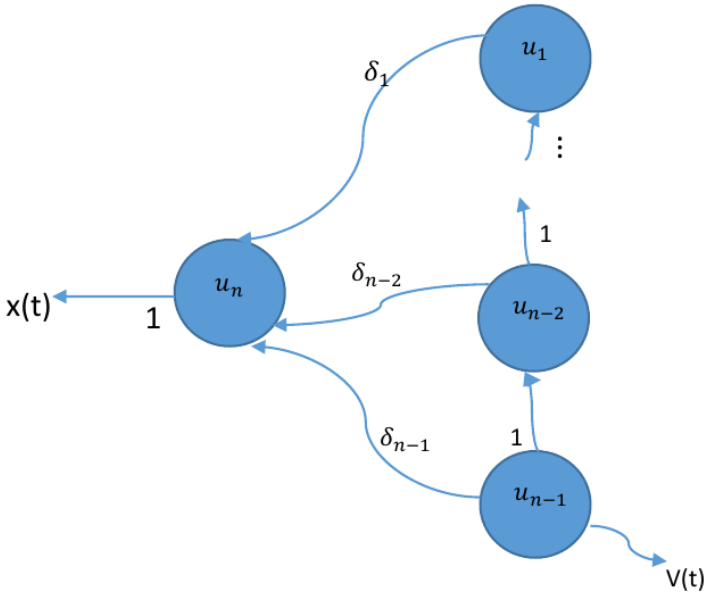

Figure 1. n-points recurrent NN.

In the diagram, $\mathbf{v}_1(\mathbf{t})$ represents the network's functioning feedback, and $\mathbf{x}(\mathbf{t})$ represents the output of the network. This persistent structure of NNs can be represented by the following representation

framework:

$$\begin{cases} \dot{\mathbf{u}}_1(\mathbf{t}) = -\mathbf{u}_1(\mathbf{t}) + \tanh(\mathbf{u}_2(\mathbf{t})), \\ \vdots \\ \dot{\mathbf{u}}_{\mathbf{n}-1}(\mathbf{t}) = -\mathbf{u}_{\mathbf{n}-1}(\mathbf{t}) + \mathbf{v}(\mathbf{t}), \\ \dot{\mathbf{u}}_{\mathbf{n}}(\mathbf{t}) = -\mathbf{u}_{\mathbf{n}}(\mathbf{t}) + \sum\limits_{i=1}^{\mathbf{n}-1} \delta_i \tanh\left(\mathbf{u}_i(\mathbf{t})\right), \\ \mathbf{x}(\mathbf{t}) = \tanh\left(\mathbf{u}_{\mathbf{n}-1}(\mathbf{t})\right), \end{cases} \tag{2.1}$$

where $\mathbf{u}(\mathbf{t}) \in \mathbb{R}^{\mathbf{n}}$ is an operational factor, and $\delta_i \in \mathbb{R},\ \ i = 1, ..., \mathbf{n}-1$ are the system's criteria or weights.

Further considerations of dynamic behaviors associated with the three-node structure of (2.1) are presented in [40] and [41], which are easily explained using a closed circuit, that is, replacing $\mathbf{v}(\mathbf{t})$ with $\mathbf{x}(\mathbf{t})$ by

$$\begin{cases} \dot{\mathbf{u}}_1(\mathbf{t}) = -\mathbf{u}_1(\mathbf{t}) + \tanh\left(\mathbf{u}_2(\mathbf{t})\right), \\ \dot{\mathbf{u}}_2(\mathbf{t}) = -\mathbf{u}_2(\mathbf{t}) + \tanh\left(\mathbf{u}_3(\mathbf{t})\right), \\ \dot{\mathbf{u}}_3(\mathbf{t}) = -\mathbf{u}_3(\mathbf{t}) + \delta_1 \tanh\left(\mathbf{u}_1(\mathbf{t})\right) + \delta_2 \tanh\left(\mathbf{u}_2(\mathbf{t})\right). \end{cases} \tag{2.2}$$

Xiao et al. [42] presented the recurrent NNs model in the Caputo fractional derivative ${}^{c}\mathbf{D}^{\phi}$ sense as follows:

$$\begin{cases} {}^{c}\mathbf{D}^{\phi_1}\mathbf{u}_1(\mathbf{t}) = -\mathbf{u}_1(\mathbf{t}) + \tanh\left(\mathbf{u}_2(\mathbf{t})\right), \\ {}^{c}\mathbf{D}^{\phi_2}\mathbf{u}_2(\mathbf{t}) = -\mathbf{u}_2(\mathbf{t}) + \tanh\left(\mathbf{u}_3(\mathbf{t})\right), \\ {}^{c}\mathbf{D}^{\phi_3}\mathbf{u}_3(\mathbf{t}) = -\mathbf{u}_3(\mathbf{t}) + \delta_1 \tanh\left(\mathbf{u}_1(\mathbf{t})\right) + \delta_2 \tanh\left(\mathbf{u}_2(\mathbf{t})\right), \end{cases} \tag{2.3}$$

where $\phi_i \in (0, 1],\ \ i = 1, 2, 3$. The framework (2.3) has $\mathbb{Z}$-symmetry, which means it is indistinguishable with regards to the modification $\mathbb{T} : (\mathbf{u}_1, \mathbf{u}_2, \mathbf{u}_3) \mapsto (-\mathbf{u}_1, -\mathbf{u}_2, -\mathbf{u}_3)$. As a result, the IC $\mathbf{O}(0, 0, 0)$ is perpetually present a state of equilibrium $\forall\ \delta_i \in \mathbb{R},\ i = 1, 2$.

We create an innovative DFNN system via undamped resonances by replacing the Caputo derivative ${}^{c}\mathbf{D}^{\phi}$ with the difference operator ${}^{c}\Delta_{\mathbf{b}}^{\phi}$ in (2.3). The graphical representation of the fractional recurrent NN simulation is written in the format that follows:

$$\begin{cases} {}^{c}\Delta_{\mathbf{b}}^{\phi}\mathbf{u}_1(\ell) = -\mathbf{u}_1(\ell - 1 + \phi) + \tanh\left(\mathbf{u}_2(\ell - 1 + \phi)\right), \\ {}^{c}\Delta_{\mathbf{b}}^{\phi}\mathbf{u}_2(\ell) = -\mathbf{u}_2(\ell - 1 + \phi) + \tanh\left(\mathbf{u}_3(\ell - 1 + \phi)\right), \\ {}^{c}\Delta_{\mathbf{b}}^{\phi}\mathbf{u}_3(\mathbf{t}) = -\mathbf{u}_3(\ell - 1 + \phi) + \delta_1 \tanh\left(\mathbf{u}_1(\ell - 1 + \phi)\right) + \delta_2 \tanh\left(\mathbf{u}_2(\ell - 1 + \phi)\right). \end{cases} \tag{2.4}$$

We focus $\phi \in (0, 1],\ \ell \in \mathbb{N}_{\mathbf{b}+1-\phi},\ \ \mathbb{N}_{\mathbf{b}} = \{\mathbf{b}, \mathbf{b}+1, \mathbf{b}+2, ...\}$ such that $\mathbf{b} \in \mathbb{R}$. ${}^{c}\Delta_{\mathbf{b}}^{\phi}$ is the Caputo-like difference operator, which can be described by [26] as

$${}^{c}\Delta_{\mathbf{b}}^{\phi}F(\ell) = \Delta_{\mathbf{b}}^{-(J-\phi)}\Delta^{J}F(\ell) = \frac{1}{\Gamma(J-\phi)} \sum_{\ell=J}^{\ell-(J-\phi)} (\ell - \tau - 1)^{(J-1\phi)}\Delta^{J}F(\tau), \tag{2.5}$$

where $\ell \in (\mathbb{N})_{\mathbf{b}+J-\phi}$ and $J = \lceil\phi\rceil + 1$. $\Delta_{\mathbf{b}}^{-\phi}$ represents the ϕ^{th} fractional sum, which can be described by [25] as

$$\Delta_{\mathbf{b}}^{\phi}F(\ell) = \frac{1}{\Gamma(\phi)} \sum_{\tau=0}^{\ell-\phi} (\ell - \tau - 1)^{(\phi-1)}F(\tau),\ \ \ell \in (\mathbb{N})_{J-\phi},\ \ \phi > 0. \tag{2.6}$$

To look into the intricate structure of the DFNN model (2.4), we will deliver the following lemma, which will allow us to obtain the computation procedure for the DFNN system (2.4):

Lemma 2.1. *[31] The solution of the initial value problem*

$$\begin{cases} {}^{c}\Delta_{\mathbf{b}}^{\phi} F(\ell) = g_1(\ell - 1 + \phi, F(\ell - 1 + \phi)), \\ \Delta^{J} F(\mathbf{b}) = F_{\mathbb{k}}, \quad \mathbf{n} = [\phi] + 1, \ \ \mathbb{k} = 0, 1, ..., \mathbf{n} - 1, \end{cases} \tag{2.7}$$

is expressed as

$$F(\ell) = F_0(\mathbf{b}) + \frac{1}{\Gamma(\phi)} \sum_{\tau=\mathbf{b}+\mathbf{n}-\phi}^{\ell-\phi} (\ell - 1 - \tau)^{(\phi-1)} g_1(\tau - 1 + \phi, F(\tau - 1 + \phi)), \ \ \tau \in \mathbb{N}_{\mathbf{b}+\mathbf{n}},$$

where

$$F_0(\mathbf{b}) = \sum_{\mathbb{k}=0}^{\mathbf{n}-1} \frac{(\ell - \mathbf{b})^{\mathbb{k}}}{\Gamma(J + 1)} \Delta^{\mathbb{k}} F(\mathbf{b}).$$

Remark 2.1. *Choose* $\mathbf{b} = 0$, *since* $(\ell - 1 - \tau)^{(\phi-1)} = \frac{\Gamma(\ell-\tau)}{\Gamma(\ell+1-\tau-\phi)}$ *and for* $J = \tau + \phi - 1$ *and* $\mathbf{n} = 1$. *For* $0 < \phi \leq 1$, *the corresponding numerical Eq* (2.7) *can be constructed as outlined below:*

$$F(\ell) = F(0) + \frac{1}{\Gamma(\phi)} \sum_{J=0}^{\ell-1} \frac{\Gamma(\ell - 1 - J + \phi)}{\Gamma(\ell - J)} g_1(J, F(J)).$$

Recall the result of the stability of the FO map.

Lemma 2.2. *[43] Assume that* $\mathbf{u}_1(\ell) = (\mathbf{u}_{11}(\ell), ..., \mathbf{u}_{1\mathbf{n}}(\ell))^{\mathbf{T}}$ *and* $\mathcal{Q} \in \mathcal{W}_{\mathbf{n}}(\mathbb{R})$. *The zero fixed point of the dynamical DFO system:*

$${}^{c}\Delta_{\mathbf{b}}^{\phi} \mathbf{u}_1(\ell) = \mathcal{Q}\, \mathbf{u}_1(\ell - 1 + \phi), \ \ \forall\ \ell \in \mathbb{N}_{\mathbf{b}+1-\phi}$$

is asymptotically stable if $\varphi_i \in \left\{\theta \in \mathbb{C} : |\phi| < (2\cos\frac{|\arg\theta|-\pi}{2-\phi})^{\phi} \ \ |\arg\phi| > \phi\pi/2\right\}$, *where* φ_i *indicates the eigenvalues of* $\mathcal{Q}$.

The stability region is presented in the following.

Lemma 2.3. *[44] Assume that the FO values* $\phi_i \in (0, 1], \ \ i = 1, ..., \mathbf{n}$. *Consider* $\mathcal{W}$ *to be the least common multiple of the denominators. the* $\mathbf{v}_i$*'s of* ϕ_i*'s, where* $\phi_i = \tau_i/\mathbf{v}_i$, $(\mathbf{v}_i, \tau_i) = 1$, $\mathbf{v}_i, \tau_i \in \mathbb{Z}^+$, $\forall\ i = 1, ..., \mathbf{n}$. *Then, the fixed point is locally asymptotically stable (LAS) if all the solutions of the equation:*

$$\det\left(\begin{bmatrix} \varphi^{\mathcal{W}\phi_1} & & 0 \\ & \ddots & \\ 0 & & \varphi^{\mathcal{W}\phi_{\mathbf{n}}} \end{bmatrix} - \mathcal{J}\right) = 0,$$

fulfill $|\arg(\varphi)| > \pi/2\mathcal{W}$, *where* $\mathcal{J}$ *is the Jacobian matrix corresponding to at the fixed point.*

3. Qualitative analysis of the DFNNs

The evolution of the DFNN designs (2.4) with undamped oscillations will be investigated in two scenarios in this section: commensurate order and incommensurate order. These tests will be carried out employing a variety of numerical modeling approaches, including phase illustrations, bifurcation schematics and MLEs predictions. The Jacobian matrix technique [31] can be used for determining the MLEs of the attractors of the DFNN model (2.4).

3.1. Commensurate order for DFNNs

We will examine the behavior of the commensurate DFNN system (2.4) in the following subsections. We are going to look over the features of the suggested commensurate DFNN framework (2.4). It needs to be mentioned that a collection of formulae in commensurate order is an ensemble of computations using similar directives. Given this, we shall subsequently present the computation technique generated by Lemma 2.1 outlined below:

$$\begin{cases} \mathbf{u}_1(\ell+1) = \mathbf{u}_1(0) + \sum\limits_{j=0}^{\mathbf{n}} \frac{\Gamma(\ell-1-j+\phi)}{\Gamma(\phi)\Gamma(\ell-j)}\big(-\mathbf{u}_1(j) + \tanh(\mathbf{u}_2(j))\big), \\ \mathbf{u}_2(\ell+1) = \mathbf{u}_2(0) + \sum\limits_{j=0}^{\mathbf{n}} \frac{\Gamma(\ell-1-j+\phi)}{\Gamma(\phi)\Gamma(\ell-j)}\big(-\mathbf{u}_2(j) + \tanh(\mathbf{u}_3(j))\big), \\ \mathbf{u}_3(\ell+1) = \mathbf{u}_2(0) + \sum\limits_{j=0}^{\mathbf{n}} \frac{\Gamma(\ell-1-j+\phi)}{\Gamma(\phi)\Gamma(\ell-j)}\big(-\mathbf{u}_3(j) + \delta_1\tanh(\mathbf{u}_1(j)) + \delta_2\tanh(\mathbf{u}_2(j))\big), \end{cases} \tag{3.1}$$

where $\mathbf{u}_1(0), \mathbf{u}_2(0),\ \mathbf{u}_3(0)$ are the ICs. For adjusting the system's specification, we write the Jacobian matrix of system (3.1) at $\mathbf{u}_1 = 0$ as

$$\mathcal{J} = \begin{pmatrix} -1 & 1 & 0 \\ 0 & -1 & 1 \\ \delta_1 & \delta_2 & -1 \end{pmatrix} \tag{3.2}$$

with the characteristic polynomial

$$\wp(\varphi) = \varphi^3 + 3\varphi^2 + (3-\delta_2)\varphi + (1-\delta_1-\delta_2). \tag{3.3}$$

Consider the nature of the roots of cubic polynomial $\wp(\varphi)$ based on $\tilde{D} = 4\delta_2^3 - 27\delta_1^2$. According to [40], Eq (3.3) has three real zeros when $\tilde{D} > 0$, but it has, a real zero and a couple of imaginary zeros when $\tilde{D} < 0$.

In this particular instance, we provide an accurate solution and provide more comprehensive evidence. For (3.3), we have the subsequent outcomes.

(i) Observe that $\delta_1 \in (-2, 2)$ and $\tilde{D} > 0$. It is simple to comprehend that $2\delta_2 - \delta_1 < 8$. According to the widely recognized Routh-Hurwitz specifications [45], alongside $\delta_2 < 1 - \delta_1$, (3.3) has three branches with negative real components. Furthermore, (3.3) possesses three valid roots when $\tilde{D} > 0$. As a result, we have

(ii) when $\tilde{D} > 0$, (3.3) possesses three real zeros $\varphi_1,\ \varphi_2$ and φ_3. Because $\lim\limits_{\varphi\mapsto\infty} \wp(\varphi) = \infty$ and $\wp(0) = 1 - (\delta_1 + \delta_2)$, we determine that $\wp(\varphi)$ possesses not less than one non-negative zero φ_1. Furthermore, remember that $\varphi_1 + \varphi_2 + \varphi_3 + 3 = 0$ and $\varphi_1\varphi_2\varphi_3 = \delta_1 + \delta_2 - 1 > 0$. It is simple to notice that $\varphi_2 + \varphi_3 < 0$ and $\varphi_2\varphi_3 > 0$, indicating that $\varphi_2 < 0$ and $\varphi_3 < 0$.

(iii) When $\tilde{D} > 0$, $\wp(\varphi)$ possesses three real zeros $\varphi_1,\ \varphi_2$ and φ_3. Observing that $\lim_{\varphi\mapsto-\infty} \wp(\varphi) = -\infty$ and $\wp(0) = 1 - (\delta_1 + \delta_2) > 0$, we can conclude that (3.3) contains not less than a single negative zero φ_1. It is worth noting that $\varphi_1\varphi_2 + \varphi_3\varphi_2 + \varphi_1\varphi_3 = 3 - \delta_2 < 0$ and $\varphi_1\varphi_2\varphi_3 = \delta_1 + \delta_2 - 1 < 0$. Afterwards we find that $\varphi_2 + \varphi_3 > 0$ and $\varphi_2\varphi_3 > 0$, which implies that $\varphi_2 > 0$ and $\varphi_3 > 0$.

(iv) When $\tilde{D} < 0$, (3.3) includes an real zero and a pair of conjugate imaginary zeros. According to the Routh-Hurwitz threshold [45], (3.3) includes three roots via non-positive real components when $\delta_1 < 1 - \delta_2$ and $2\delta_2 < 8 + \delta_1$. As a result, an assertion **(iv)** implies immediately.

(v) When $\tilde{D} < 0$, (3.3) includes a non-positive real root and a pair of conjugate imaginary zeros. According to the Routh-Hurwitz threshold [45], (3.3) includes the root via non-positive real components when $2\delta_2 > 8 + \delta_1$.

(vi) When $\tilde{D}(\varphi < 0)$, (3.3) includes an real zero φ_1 and an additional set of conjugate complex zeros $\varphi_{2,3}$. Given that $\lim_{\varphi\mapsto\infty} \wp(\varphi) = \infty$ and $\wp(0) = 1 - (\delta_1 + \delta_2) < 0$, we determine that $\varphi_1 > 0$. Notice that $+\varphi_1 + \varphi_2 + \varphi_3 + 3 < 0$. As we observe, $\varphi_2 + \varphi_3 < 0$. As a consequence, φ_2 and φ_3 are imaginary roots with no real components.

Remark 3.1. *According to the above assertions, we are able to observe that (δ_1, δ_2)-space can be split into six segments for the curve $\tilde{D} > 0$ and the lines $\delta_2 = 1 - \delta_1,\ \delta_2 = (\delta_1/2) + 4$ and $\delta_2 < 3$ with the specifications of roots $\varphi_1,\ \varphi_2$ and φ_3 as follows:*

$$\begin{aligned}
\Upsilon_1 &:= \{(\delta_1, \delta_2)\big|\tilde{D} < 0,\ \delta_2 > \delta_1/2 + 4,\ \varphi_1 < 0,\ \varphi_{2,3} = \varrho \pm j\Bbbk\ (\varrho > 0)\},\\
\Upsilon_2 &:= \{(\delta_1, \delta_2)\big|\tilde{D} < 0,\ \delta_2 < 1 - \delta_1,\ \delta_2 < \delta_1/2 + 4,\ \varphi_1 < 0,\ \varphi_{2,3} = \varrho \pm j\Bbbk\ (\varrho < 0)\},\\
\Upsilon_3 &:= \{(\delta_1, \delta_2)\big|\tilde{D} > 0,\ \delta_2 < 1 - \delta_1,\ \delta_2 < 3,\ \varphi_{1,2,3} < 0\},\\
\Upsilon_4 &:= \{(\delta_1, \delta_2)\big|\tilde{D} < 0,\ \delta_2 > 1 - \delta_1,\ \varphi_1 > 0,\ \varphi_{2,3} = \varrho \pm j\Bbbk\ (\varrho < 0)\},\\
\Upsilon_5 &:= \{(\delta_1, \delta_2)\big|\tilde{D} > 0,\ \delta_2 > 1 - \delta_1,\ \varphi_1 > 0,\ \varphi_{2,3} < 0\},\\
\Upsilon_6 &:= \{(\delta_1, \delta_2)\big|\tilde{D} < 0,\ \delta_2 < 1 - \delta_1,\ \delta_2 > 3,\ \varphi_1 < 0,\ \varphi_{2,3} > 0\}.
\end{aligned}$$

Proposition 3.1. *Assume that settings $\Omega_i = 108\delta_1 \pm \sqrt{11664\delta_1^2 - 1728\delta_2^3}$, for $i = 1, 2$ have been supplied by the model* (3.1) *and then the subsequent results hold:*
(a_1) When $(\delta_1, \delta_2) \in \Upsilon_2 \cup \delta_3$, fixed point $\mathbf{u}_1 = 0$ of framework (3.1) *is LAS for all $0 < \phi \leq 1$.*
(a_2) When $(\delta_1, \delta_2) \in \Upsilon_4 \cup \delta_5 \cup \Upsilon_6$, fixed point $\mathbf{u}_1 = 0$ of framework (3.1) *is unstable for all $0 < \phi \leq 1$.*
(a_3) When $(\delta_1, \delta_2) \in \Upsilon_1$ and $\arctan\left(\frac{\sqrt{3}(\sqrt[3]{\Omega_2} - \sqrt[3]{\Omega_1})}{\sqrt[3]{\Omega_1} + \sqrt[3]{\Omega_2} + 12}\right) > \phi\pi/2$, fixed point $\mathbf{u}_1 = 0$ of framework (3.1) *is LAS.*
(a_4) When $(\delta_1, \delta_2) \in \Upsilon_1$ and $\arctan\left(\frac{\sqrt{3}(\sqrt[3]{\Omega_2} - \sqrt[3]{\Omega_1})}{\sqrt[3]{\Omega_1} + \sqrt[3]{\Omega_2} + 12}\right) < \phi\pi/2$, then the fixed point $\mathbf{u}_1 = 0$ of framework (3.1) *is unsteady.*

Proof. In view of Remark 3.1, it is easy to see the allocation of roots of the characteristic polynomial (3.3) in (δ_1, δ_2)-space.
(a_1) When $(\delta_1, \delta_2) \in \Upsilon_2 \cup \Upsilon_3$, each of the real eigenvalues and real components of the complex conjugate eigenvalues of (3.3) are non-positive. This means that all of the eigenvalues of (3.3) are in the left-half-plane and in the steady domain (see Figure 2). As a result, the framework (3.1) possesses fixed point $\mathbf{u}_1 = 0$ which is LAS.
(a_2) When $(\delta_1, \delta_2) \in \Upsilon_4 \cup \Upsilon_5 \cup \Upsilon_6$, then (3.3) must have not less than one positive real root. As a result, framework (3.1) has fixed point $\mathbf{u}_1 = 0$ which is unsteady.

(a_3) When $(\delta_1, \delta_2) \in \Upsilon_1$, (3.3) must have a couple of imaginary eigenvalues $\varphi_{2,3}$ having non-negative real components and $\varphi_1 < 0$. Then, $\varphi_1 = \frac{\sqrt[3]{\Omega_1}+\sqrt[3]{\Omega_2}-6}{6}$ and $\varphi_{2,3} = \frac{-(\sqrt[3]{\Omega_1}+\sqrt[3]{\Omega_2})-12\pm i\sqrt{3}(\sqrt[3]{\Omega_1}-\sqrt[3]{\Omega_2})}{12}$. Therefore, simple computations yield $\left|\arg(\varphi_1)\right| = \pi > \phi\pi/2$ and $\left|\arg(\varphi_{2,3})\right| = \arctan\left(\frac{\sqrt{3}(\sqrt[3]{\Omega_2}-\sqrt[3]{\Omega_1})}{\sqrt[3]{\Omega_1}+\sqrt[3]{\Omega_2}+12}\right)$. As a result, if assertion (a_3) has its fulfilled, the fixed point $\mathbf{u}_1 = 0$ of the structure (3.1) is LAS.

(a_4) This finding is immediately connected to $\arctan\left(\frac{\sqrt{3}(\sqrt[3]{\Omega_2}-\sqrt[3]{\Omega_1})}{\sqrt[3]{\Omega_1}+\sqrt[3]{\Omega_2}+12}\right) < \phi\pi/2$. □

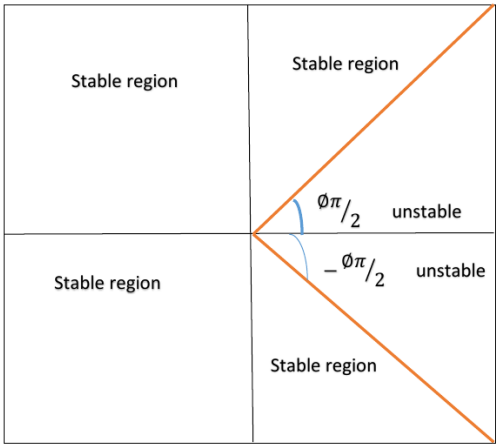

Figure 2. Stability domain for FO system when $\phi \in (0, 1)$.

Figure 3(a-c) demonstrates the fact that the configurations $\mathbf{u}_{1i}$. $i = 1, 2, 3$, of framework (3.1) are simultaneously non-increasing towards $\mathbf{u}_1 = 0$, where $(\delta_1, \delta_2) = (-1.0, 1.0) \in \Upsilon_2$, $\phi = 0.7$, and $(\delta_1, \delta_2) = (0, 0.5) \in \Upsilon_3$, $\phi = 0.8$, respectively. Furthermore, Figure 3(d-i) illustrates how the fixed point $\mathbf{O}(0, 0, 0)$ is unsteady, where $(\delta_1, \delta_2) = (2.0, 1.0) \in \Upsilon_4$ with $\phi = 0.85$, $(\delta_1, \delta_2) = (1.0, 4.0) \in \Upsilon_5$ with $\phi = 0.45$, and $(\delta_1, \delta_2) = (-5.6, 6) \in \Upsilon_6$ with $\phi = 0.25$, respectively.

In fact, the imaginary axis is generally considered to be the stability collateral of a classical mechanism. The bifurcation happens when a pair of complex conjugate eigenvalues of (3.2) assessed at the fixed point connect the imaginary axis as the bifurcation setting approaches a critical threshold, and a collection of regular methods emerge within the stable state. As stated in Remark 3.1, the equilibrium domain of DFO platforms with commensurate order is a three-dimensional surface with the apex at the origin and extending into the right half of the imaginary axis, enclosing an angle of $\pm\phi\pi/2$. In the simplest terms, $|\arg(\varphi)| = \phi\pi/2$ describes the equilibrium boundaries for such structures [46]. As a result, whenever a set of complex conjugate eigenvalues of (3.2) connect the stable limit $|\arg(\varphi)| = \phi\pi/2$, a bifurcation develops in framework (3.1), resulting in the appearance of an outgrowth of constant fluctuations derived from a stable state. It ought to be pointed out that just a handful of complex conjugate eigenvalues that have positive real components will traverse the equilibrium boundary $|\arg(\varphi)| = \phi\pi/2$, which is located in the in the complex plane's precisely split. Initially, we present the bifurcation principle over the broader DFNNs (3.1) by considering the sequence as the bifurcation setting.

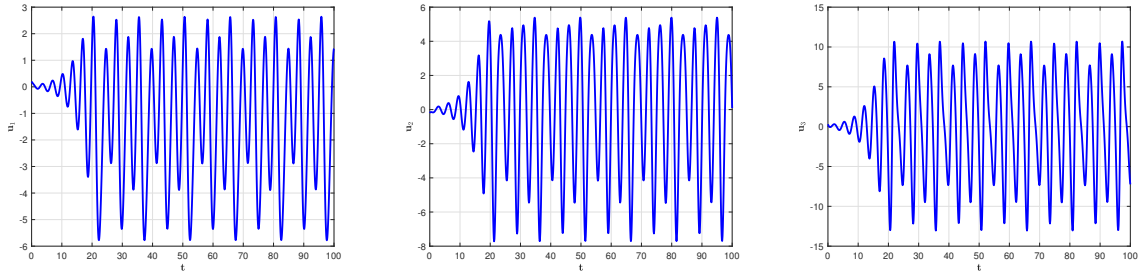

(a) $(\delta_1, \delta_2) = (-1.0, 1.0)$ *and* $\phi = 0.7$ **(b)** $(\delta_1, \delta_2) = (-1.0, 1.0)$ *and* $\phi = 0.7$ **(c)** $(\delta_1, \delta_2) = (-1.0, 1.0)$ *and* $\phi = 0.7$

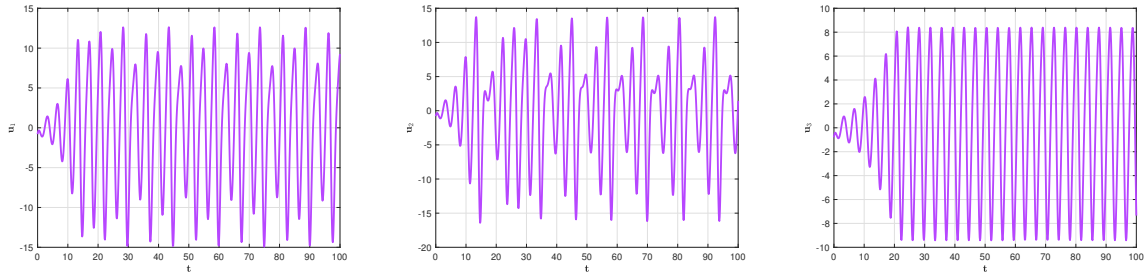

(d) $(\delta_1, \delta_2) = (2.0, 1.0)$ *and* $\phi = 0.85$ **(e)** $(\delta_1, \delta_2) = (2.0, 1.0)$ *and* $\phi = 0.85$ **(f)** $(\delta_1, \delta_2) = (2.0, 1.0)$ *and* $\phi = 0.85$

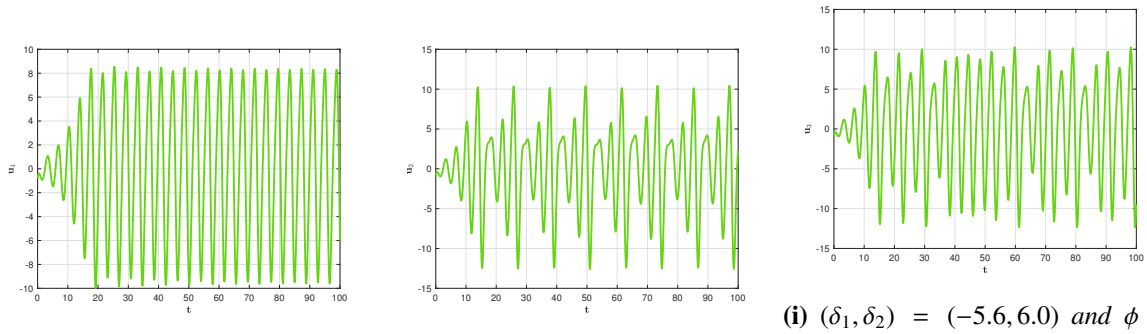

(g) $(\delta_1, \delta_2) = (1.0, 4.0)$ *and* $\phi = 0.45$ **(h)** $(\delta_1, \delta_2) = (1.0, 4.0)$ *and* $\phi = 0.45$ **(i)** $(\delta_1, \delta_2) = (-5.6, 6.0)$ *and* $\phi = 0.25$

Figure 3. Stable-state $\mathbf{u} = 0$ for commensurate order of FDNN system (3.1) is LAS with various FOs.

According to the DFO equilibrium hypothesis in [46], assuming $\phi^* = \frac{2}{\pi}|\arg(\varphi_{2,3})|$, and $\phi = \phi^*$ is the stable boundary region for the commensurate-order framework (3.1) via dimension 3. When $\phi \in (0, \phi^*)$, the couple of eigenvalues $\varphi_{2,3}$ comply with the variant $|\arg(\varphi)| > \frac{\phi\pi}{2}$. The variant $|\arg(\varphi)| > \frac{\phi\pi}{2}$ is additionally satisfied by the non-positive real eigenvalue φ_1. We comprehend via the robustness outcomes in [47] that the state of balance point $\tilde{\mathbf{u}}_1$ is equally stable. When $\phi \in (\phi^*, 1]$, two pairs of eigenvalues $\varphi_{2,3}$ fail to comply with the variant $|\arg(\varphi)| > \frac{\phi\pi}{2}$. As a result, the fixed point $\tilde{x}$ is unsteady.

Considering the results reported in [47], $|\arg(\varphi_{2,3})| = \phi^*\pi/2$ is equivalent to a bifurcation in structure (3.1). Consequently, mechanism (3.1) has a bifurcation point $\phi = \phi^*$. As it increases and passes the threshold of significance, the fixed point $\tilde{\mathbf{u}}_1$ turns unsteady, and irregular fluctuations develop in the vicinity of $\tilde{\mathbf{u}}_1$ resulting from the bifurcation trend. It is pertinent to recognize that transformation was successfully accomplished for the fixed eigenvalues $\varphi_{2,3}$ as the bifurcation setting fluctuates. Meanwhile, the structure (3.1) is considered minimally stable iff each eigenvalue of (3.2)

examined at the fixed point fulfills $|\arg(\varphi)| \geq \phi\pi/2$ and all eigenvalues fulfilling $|\arg(\varphi)| = \phi\pi/2$, possess geometric multiplicity of one [48]. As a result, with respect to the aforesaid computations, framework (3.1) alongside inner dimension three is slightly unstable. The bifurcation theory and $\eta_{\max}$ for the commensurate-order framework (3.1) via internal measurement three are illustrated in Figure 4 when $\phi \in (0, 1]$.

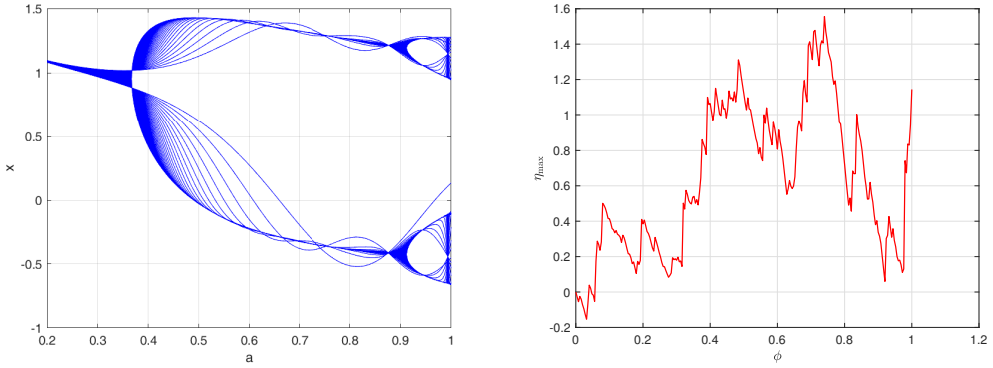

(a) $\phi = 0.75$ **(b)** $\phi = 0.75$

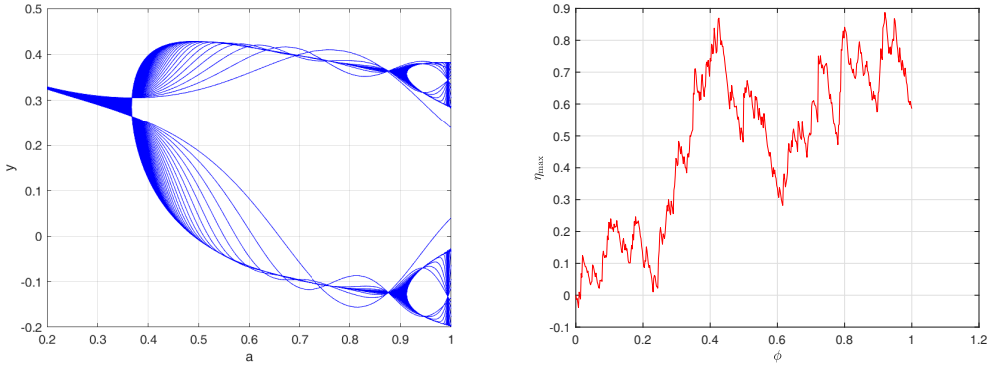

(c) $\phi = 0.80$ **(d)** $\phi = 0.80$

Figure 4. Bifurcation and MLEs plots of DFNN model (3.1) for various values of ϕ.

Using Remark 3.1, (3.3) has a couple of eigenvalues $\varphi_{2,3}$ containing non-negative real components, and $\varphi_1 < 0$, when the order $\phi^* = (2/\pi)\arctan\left(\frac{\sqrt{3}(\sqrt[3]{\Omega_2} - \sqrt[3]{\Omega_1})}{\sqrt[3]{\Omega_1} + \sqrt[3]{\Omega_2} + 12}\right)$. A bifurcation occurs in conjunction with the axis (3.1) in the classical NN [18]. Yet, the appropriate DFO framework (3.1) fails to generate a bifurcating system according to the identical conditions, as computational analyses will reveal later.

Proposition 3.1 proposes an approach for creating DFO neural oscillations by varying the DFO. In particular, framework (3.1) converges to the fixed point $\tilde{\mathbf{u}}_1$ when ϕ is less than ϕ^*, implying that no regular fluctuations develop; meanwhile the bifurcation might happen as ϕ traverses a critical point $\phi*$, in which an assortment of repeated waves bifurcates from the fixed point $\tilde{\mathbf{u}}_1$.

In mechanism (3.1), there are undamped resonances attributed to bifurcations when $(\delta_1, \delta_2, \phi) \in \Pi$, where $\Pi = \{(\delta_1, \delta_2, \phi) | (\delta_1, \delta_2) \in \Upsilon_1, \phi \in (\phi^*, 1]\}$. According to Proposition 3.1, regular fluctuations resulting from the bifurcation in framework (3.1) occur when $(\delta_1, \delta_2) \in \Upsilon_1$, where $\phi \in (\phi^*, \phi^* + \epsilon)$ demonstrates that the structure (3.1) has an uninterrupted limit process when $(\delta_1, \delta_2) \in \Upsilon_1$ and $\phi = 1$. This shows that the flexibility in selecting δ_1, δ_2 and ϕ in mechanism (3.1) enables one to figure out the

precise location and sequence of the eigenvalues, and that contributes to the resulting fluctuation. For a constant δ_1, the value $\phi(\delta_2) = (2/\pi)\arctan\left(\frac{\sqrt{3}(\sqrt[3]{\Omega_2}-\sqrt[3]{\Omega_1})}{\sqrt[3]{\Omega_1}+\sqrt[3]{\Omega_2}+12}\right)$ demonstrates the periodic and non-periodic domains for the DFNN model (3.1).

We vary the DFO to investigate the dynamic behaviors of the DFNNs (3.1) with the structure's settings (δ_1, δ_2) set to $(\delta_1, \delta_2) = (-5.0, 3.0) \in \Upsilon_1$. As a result of Remark 3.1 and $\phi^* = 0.9912$, in accordance with Proposition 3.1, when $\phi^* > \phi$, the directions merge to the ICs, as illustrated in Figure 5(a-c) and Figure 5(d-f). Meanwhile, when ϕ is increased to pass ϕ^*, the ICs are not stable and a bifurcation develops, as demonstrated in Figure 6(a-c). Additionally, considering the fluctuations in Figure 6(d-f), the dimension of framework (3.3) is 2.79. It needs to be emphasized that according to our DFO approach, the state of balance at $\mathbf{u}_1 = 0$, which is deemed unstable in the classical model (2.2), is capable of becoming extremely steady (see Figure 3). The variability of the structure's elements δ_1 and δ_2 in the DFNNs (3.1), which ensures its behavior has recurring fluctuations, is nonetheless less extensive than in the analogous classical NN (2.2).

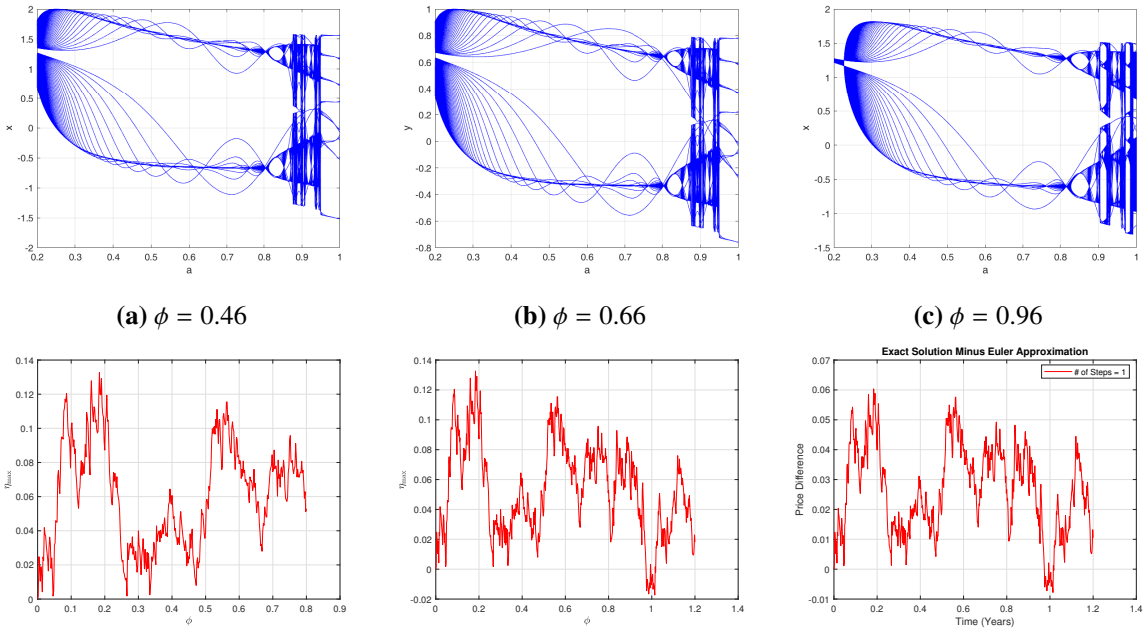

(a) $\phi = 0.46$ **(b)** $\phi = 0.66$ **(c)** $\phi = 0.96$

(d) $\phi = 0.46$ **(e)** $\phi = 0.66$ **(f)** $\phi = 0.96$

Figure 5. Bifurcation and MLEs for parametric values (δ_1, δ_2) of the DFNN system (3.1) for various DFOs.

In the following modeling, the amplitude of the supreme fluctuations is identified and contrasted to the potential value obtained in (3.2). This technique is employed for $(\delta_1, \delta_2) = (-8.0, 2.12)$ and $\phi = 0.94$, which is quite roughly equivalent to $\phi^* = 0.943$. The repetition rate is suggested to be 1.4799 rad/s, or the time frame of the oscillation needs to be 4.3456 s. Figure 3 demonstrates this aspect.

Currently, we examine computationally certain characteristics of amplitudes of oscillations in the DFNN (3.1). The process representations for the settings $(\delta_1, \delta_2) = (8.0, 2.1)$ as the DFO fluctuates from 0.56, 0.65, 0.76, 0.81, 0.90 and 0.99 are shown in Figure 6. The data demonstrates that the intensity of the fluctuations increases with greater precision [48]. Figure 3 demonstrates that the

frequency of the oscillations improves almost precisely via FO. It is apparent that the suggested commensurate DFO system displays erratic movement when the DFO drops and recurring circulation when the FO increases. These simulations using numerical methods show that the commensurate DFNN structure (3.1) has a number of captivating flexible attributes.

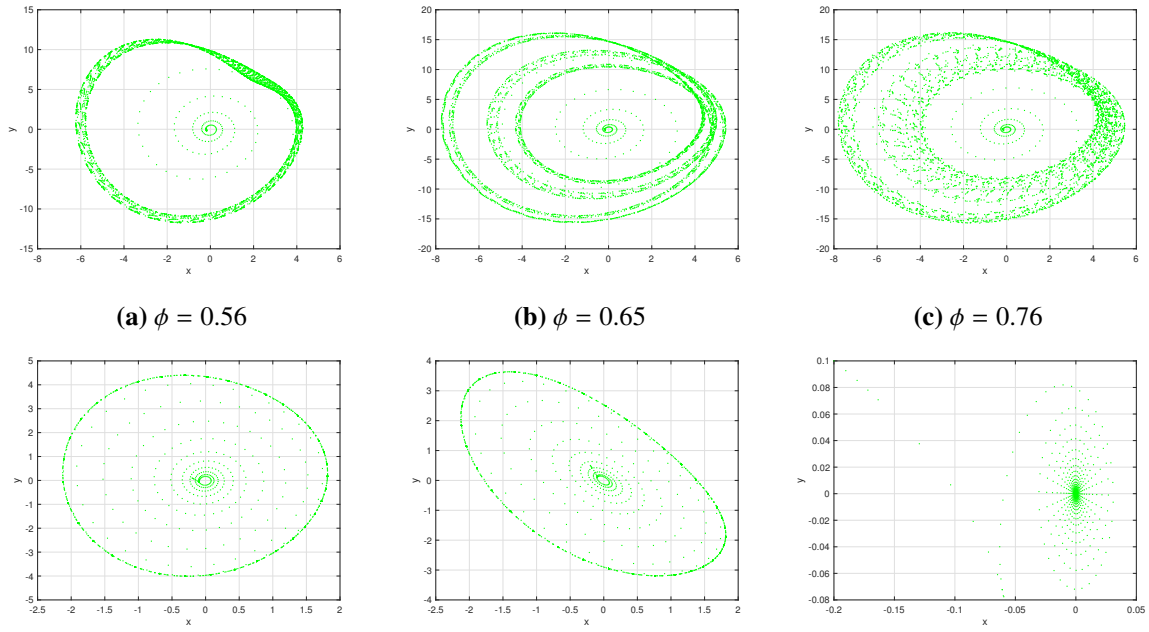

(a) $\phi = 0.56$ **(b)** $\phi = 0.65$ **(c)** $\phi = 0.76$

(d) $\phi = 0.81$ **(e)** $\phi = 0.90$ **(f)** $\phi = 0.99$

Figure 6. Phase depictions of DFNN system (3.1) for various DFOs $\phi \in (0, 1]$.

3.2. Incommensurate order DFNN system

The behavior of the NN system with incommensurate DFO measurements is investigated in this subsection. The notion of employing distinguished DFOs for every formula of the structure is referred to as the incommensurate order mechanism. The representation of the incommensurate DFNN is expressed as

$$\begin{cases} {}^{c}\Delta_{\mathbf{b}}^{\phi_1}\mathbf{u}_1(\ell) = -\mathbf{u}_1(\ell-1+\phi_1) + \tanh\left(\mathbf{u}_2(\ell-1+\phi_1)\right), \quad \forall\ \ell \in \mathbb{N}_{\mathbf{b}-\phi_1+1}, \\ {}^{c}\Delta_{\mathbf{b}}^{\phi_2}\mathbf{u}_2(\ell) = -\mathbf{u}_2(\ell-1+\phi_2) + \tanh\left(\mathbf{u}_3(\ell-1+\phi_2)\right), \quad \forall\ \ell \in \mathbb{N}_{\mathbf{b}-\phi_2+1}, \\ {}^{c}\Delta_{\mathbf{b}}^{\phi_3}\mathbf{u}_3(\ell) = -\mathbf{u}_3(\ell-1+\phi_3) + \delta_1 \tanh\left(\mathbf{u}_1(\ell-1+\phi_3)\right) + \delta_2 \tanh\left(\mathbf{u}_2(\ell-1+\phi_3)\right), \quad \forall\ \ell \in \mathbb{N}_{\mathbf{b}-\phi_3+1}, \end{cases} \tag{3.4}$$

According to Lemma 2.1, the mathematical representation of the incommensurate DFNN model (3.4) can be written as

$$\begin{cases} \mathbf{u}_1(\ell+1) = \mathbf{u}_1(0) + \sum\limits_{j=0}^{\mathbf{n}} \frac{\Gamma(\ell-1-j+\phi_1)}{\Gamma(\phi_1)\Gamma(\ell-j)}\big(-\mathbf{u}_1(j) + \tanh(\mathbf{u}_2(j)\big), \\ \mathbf{u}_2(\ell+1) = \mathbf{u}_2(0) + \sum\limits_{j=0}^{\mathbf{n}} \frac{\Gamma(\ell-1-j+\phi_2)}{\Gamma(\phi_2)\Gamma(\ell-j)}\big(-\mathbf{u}_2(j) + \tanh(\mathbf{u}_3(j)\big), \\ \mathbf{u}_3(\ell+1) = \mathbf{u}_2(0) + \sum\limits_{j=0}^{\mathbf{n}} \frac{\Gamma(\ell-1-j+\phi_3)}{\Gamma(\phi_3)\Gamma(\ell-j)}\big(-\mathbf{u}_3(j) + \delta_1 \tanh(\mathbf{u}_1(j)) + \delta_2 \tanh(\mathbf{u}_2(j)\big), \quad \ell = 1, 2, \ldots . \end{cases} \tag{3.5}$$

The dynamic matrix of the incommensurate DFNN model (3.5) with logical internal directives can be demonstrated to have the indicative equation (3.4). The robustness range for the incommensurate-order model (3.5) is given by $|\arg(\varphi)| = \pi/2M_1$, where M_1 is the lowest common multiple of the inner order denominators.

Take into account the incommensurate DFNN (3.5) using DFOs as a particular case. For this, DFOs are assumed to be $\phi_1 = \phi_2 = \mathfrak{I}/(2\mathfrak{I}+1)$ and $\phi_3 = 2\mathfrak{I}/(2\mathfrak{I}+1)$, where $\mathfrak{I} \in \mathbb{N}$. In this scenario, the characteristic polynomial of the expression (3.3) is:

$$\varphi^{4\mathfrak{I}} + 2\varphi^{3\mathfrak{I}} + 2\varphi^{2\mathfrak{I}} + (2-\delta_2)\varphi^{\mathfrak{I}} + (1-\delta_1-\delta_2) = 0. \tag{3.6}$$

Plugging $w_1 = \varphi^{\mathfrak{I}}$ into (3.6), it reduces to

$$w_1^4 + 2w_1^3 + 2w_1^2 + (2-\delta_2)w_1 + (1-\delta_1-\delta_2) = 0. \tag{3.7}$$

If δ_1 and δ_2 are determined to ensure that (3.7) possesses a pair of solutions $\jmath\exp(\pm\mathbb{k}\mathfrak{I}\pi/2(2\mathfrak{I}+1))$, where $\jmath$ is non-negative, then two roots of (3.6), i.e., $\jmath\exp(\pm\mathbb{k}\pi/2(2\mathfrak{I}+1))$ will be on the boundary of stability $|\arg(\varphi)| = \pi/2(2\mathfrak{I}+1)$ and its additional bases can be decided in the steady domain $|\arg(\varphi)| > \pi/2(2\mathfrak{I}+1)$. As a result, framework (3.5) will remain relatively steady in the present instance. Whenever the set of eigenvalues $\jmath\exp(\pm\mathbb{k}\pi/2(2\mathfrak{I}+1))$, traverse the steady-state region $|\arg(\varphi)| = \pi/2(2\mathfrak{I}+1)$ as the settings δ_1 and δ_2 evolve, a bifurcation occurs, and a group of recurring fluctuations emerges via the initial state $\mathbf{u}_1 = 0$. We examine framework (3.5) considering the simple scenario $\mathfrak{I} = 1$, that is, $(\phi_1, \phi_2, \phi_3) = (0.5, 0.5, 0.65)$. By restricting δ_1 and δ_2, the intention is to set up a set of eigenvalues in the steady domain to traverse the boundary of stability $|\arg(\varphi)| = \pi/6$ and penetrate the area of unpredictability. When $(\delta_1, \delta_2) = (-70, 29)$, the corresponding formula (3.6) has two distinct sets of imaginary roots: $\varphi_{1,2} = 1.5 \pm 0.867\mathbb{k}$ on the equilibrium region $|\arg(\varphi)| = \pi/6$ and $\varphi_{3,4} = 2.5 \pm 2.78388\mathbb{k}$ in the steady domain $|\arg(\varphi)| = \pi/6$. The eigenvalue pattern (3.6) for $(\phi_1, \phi_2, \phi_3) = (0.5, 0.5, 0.65)$ and $\delta_1 = -70$ to be δ_2 fluctuates from 30 to 37 and is shown in Figure 7(a). When δ_2 changes, $\varphi_{3,4}$ stays within the steady region, whereas $\varphi_{1,2}$ traverses the zone of the stability limit.

We alter the setting δ_2 to examine the dynamic practices of the incommensurate-order framework (3.5), considering the selected directives $(\phi_1, \phi_2, \phi_3) = (1, 1, 0.85)$, and the setting δ_2. According to the preceding debate, $\delta_2^* = 29$ is the crucial number for mechanism (3.5). As illustrated by Figure 7(b), the configurations $\mathbf{u}_{1i}$ $(i = 1, 2, 3)$ of framework (3.5) decrease asynchronously towards the ICs when $\delta_2 < \delta_2^*$. As δ_2 increases as it proceeds within δ_2^*, its starting point becomes unstable and a bifurcation develops, as illustrated in Figure 7(b). To identify the waveform shown in Figure 7(b), the efficient measurement of the framework (3.5) is 4/3.

The authors of [47] demonstrated that for DFO linear frameworks, every combination of complex eigenvalues $\varphi_{1,2}$ agreed on a stable margin $|\arg(\varphi)| = \pi/2M_1$ is equivalent to recurring fluctuations via regularity $|\varphi_{1,2}|^{M_1}$. When $(\phi_1, \phi_2, \phi_3) = (0.5, 0.8, 0.65)$, and $\delta_1 = -70$, the periodicity is equivalent to $|\varphi_{1,2}|^{M_1} = 3\sqrt{3}$ rad/s, or the duration of the fluctuation is 2.0012 s when δ_2 is approximately equal to δ_2^*. The result is supported by Figure 7(c).

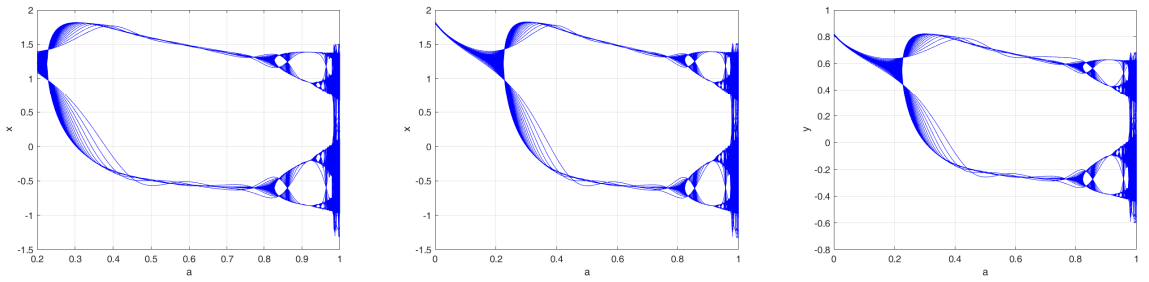

(a) $(\phi_1, \phi_2, \phi_3) = (0.5, 0.5, 0.65)$ **(b)** $(\phi_1, \phi_2, \phi_3) = (1, 1, 0.85)$ **(c)** $(\phi_1, \phi_2, \phi_3) = (0.5, 0.8, 0.65)$

Figure 7. Bifurcation plots for DFNN model (3.4) via the system parametric representations (δ_1, δ_2) and (ϕ_1, ϕ_2, ϕ_3).

The phase depictions of the framework (3.5) about (ϕ_1, ϕ_2, ϕ_3) and $\delta_1 = -70$ as the mechanism attribute δ_2 fluctuates from 35.1, 33.5, 33.4, 33.3, 33.2 and 32.0, respectively, are shown in Figure 8. This graph shows how the intensity of the fluctuations increases as δ_2 increases. The influence of δ_2 on the strength of the chaos is depicted in Figure 8.

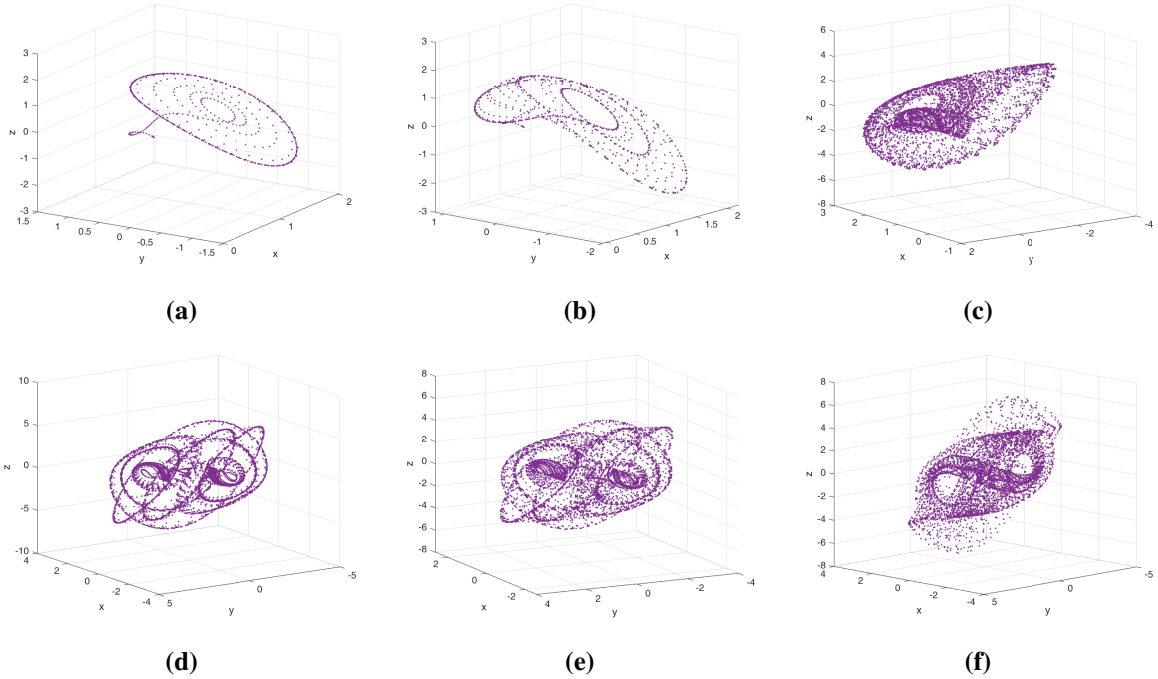

(a) **(b)** **(c)**

(d) **(e)** **(f)**

Figure 8. Phase depictions for DFNN (3.5) for various parametric values (δ_1, δ_2) and (a) $(\phi_1, \phi_2, \phi_3) = (0.7, 1, 1)$,(b) $(\phi_1, \phi_2, \phi_3) = (0.1, 0.7, 1)$,(c) $(\phi_1, \phi_2, \phi_3) = (0.9, 0.4, 0.6)$,(d) $(\phi_1, \phi_2, \phi_3) = (0.6, 0.9, 1)$,(e) $(\phi_1, \phi_2, \phi_3) = (0.9, 1, 0.9)$,(f) $(\phi_1, \phi_2, \phi_3) = (1, 0.7, 1)$.

The several bifurcation and MLEs schematics in Figure 9 indicate the patterns of the incommensurate simulation by ranging $(\delta_1, \delta_2) = (-70, 30)$ and the ICs $(\mathbf{u}_1(0), \mathbf{u}_2(0), \mathbf{u}_2(0)) = (0.01, -0.01, 0.01)$. The aforementioned graphs are clearly distinct, demonstrating that changes in DFOs ϕ_1, ϕ_2 and ϕ_3 have an effect on the stages of the incommensurate DFNN system (3.5).

For example, for $(\phi_1, \phi_2, \phi_3) = (0.9, 1, 1)$, we recognize that the structure develops from erratic to irregular as the parameter setting improves. The chaos is apparent during the range of values for $(\phi_1, \phi_2, \phi_3) = (0.9, 0.4, 1)$, excluding a restricted area when δ_2 addresses 30.1, whereas for $(\phi_1, \phi_2, \phi_3) = (0.7, 1, 0.9)$, while the value of δ_2 improves and within 30.3, the incommensurate DFNN system (3.5) demonstrates recurring zones with five-period orbital positions. In addition, we examine a number of additional scenarios to provide an improved representation of the impact of incommensurate orders on the DFNN model's (3.5) practices.

Here, we alter the DFO ϕ_1 from 0 to 1 using an incremental size of $\Delta\phi_1 = 0.005$. Figure 9(a) and (b) demonstrate the bifurcation and their associated MLEs for $\phi_2 = \phi_3 = 1$, the other specified values $(\delta_1, \delta_2) = (-8, 2.1)$ and the ICs $(\mathbf{u}_1(0), \mathbf{u}_2(0), \mathbf{u}_3(0)) = (0.2, -0.2, 0.3)$. According to Figure 9, the configuration of the incommensurate DFNN (3.5) exhibits chaotic behavior for a DFO ϕ_1, as evidenced by non-negative MLEs, which are illustrated in Figure 9. For the DFO ϕ_1 close to 1, the $\eta_{\max}$ demonstrated in Figure 9(a) and (b) alternates within the two extremes. As an outcome of the emergence of certain recurring patterns, a chaotic scene is observed.

The bifurcation and its $\eta_{\max}$ are depicted in Figure 9(c) and (d) to investigate the fluctuating behaviors of the incommensurate DFNN system (3.5) when ϕ_2 is a configurable factor. These outcomes are achieved by ranging ϕ_2 in the range $(0, 1]$ and with incommensurate DFOs $\phi_1 = 0.9$ and $\phi_3 = 1$, respectively. The other specified values $(\delta_1, \delta_2) = (-8, 2.1)$ and the ICs $(\mathbf{u}_1(0), \mathbf{u}_2(0), \mathbf{u}_3(0)) = (0.2, -0.2, 0.3)$ have stayed unaffected. We understand that when the DFO ϕ_2 is inadequate, pathways remain steady. When ϕ_2 rises, chaotic behaviors tend to be observed at which the real values of $\eta_{\max}$ are non-negative, and inadequate recurring zones can be observed in which the measures of $\eta_{\max}$ are positive. Furthermore, as ϕ_2 grows bigger and eventually reaches 1, the MLE's measurements vary from non-negative to negative, implying that the pathways of the incommensurate DFNN system (3.5) transition from erratic to periodic.

We generate the bifurcation visualization and $\eta_{\max}$ of the offered novel incommensurate DFNN system (3.5) rather than $\phi_3 \in (0, 1]$ and choose the incommensurate DFOs as $\phi_1 = 0.4$ and $\phi_2 = 1$. As compared to the preceding instances, the pathways of the incommensurate designs are chaotic in Figure 9(e) and (f) when the DFO ϕ_3 necessitates higher numbers closer to 1 while $\eta_{\max}$ requires its greatest magnitude. The routes stabilize. Furthermore, as ϕ_3 reduces, the steady region and recurring views become apparent. Whenever the incommensurate FO ϕ_3 decreases more dramatically, chaotic practices reappear in $\phi_3 \in (0.3010, 0.6010)$. When the DFO decreases near zero, insurrection vanishes, and recurring views along with four-period revolves develop in which the outcomes of $\eta_{\max}$ are negative. Improvements in the incommensurate DFOs, corresponding to the aforementioned outcomes, possess an influence on the fluctuating characteristics of a DFNN system (3.5) with undamped oscillations. Additionally, it indicates that incommensurate DFOs might appropriately symbolizes the structure's patterns, as evidenced through the sequential depictions of the configuration factors of the incommensurate DFNN system (3.5) shown in Figure 9(g) and (h).

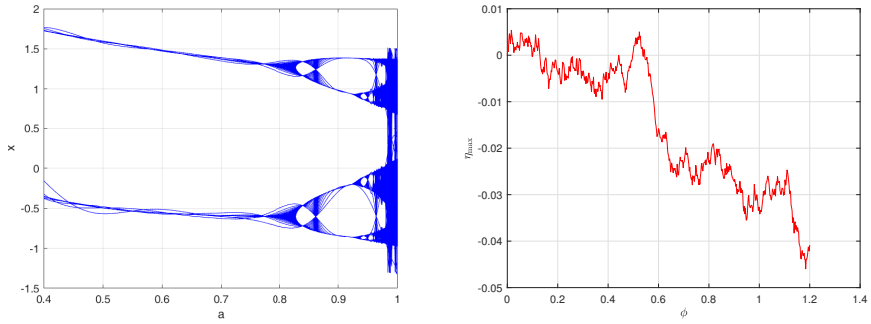

(a) $(\phi_1, \phi_2, \phi_3) = (0.7, 1, 1)$ **(b)** $(\phi_1, \phi_2, \phi_3) = (0.7, 1, 1)$

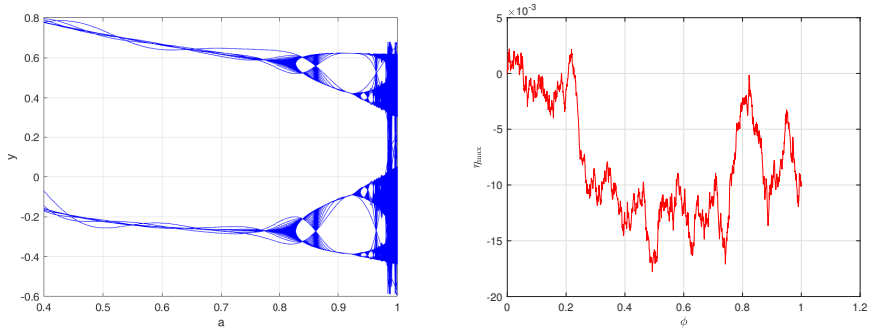

(c) $(\phi_1, \phi_2, \phi_3) = (0.9, 0.6, 1)$ **(d)** $(\phi_1, \phi_2, \phi_3) = (0.9, 0.6, 1)$

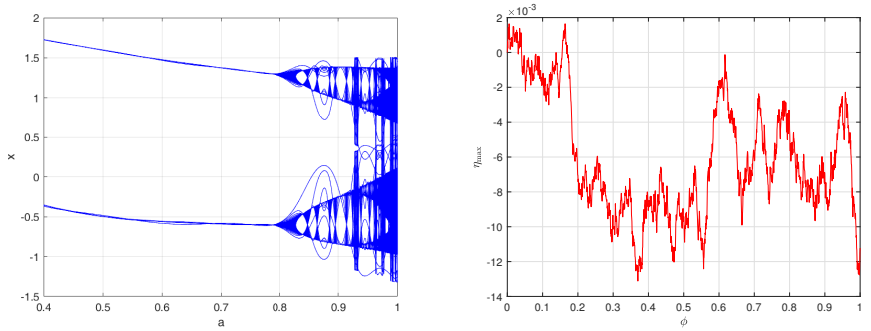

(e) $(\phi_1, \phi_2, \phi_3) = (0.4, 1, 0.65)$ **(f)** $(\phi_1, \phi_2, \phi_3) = (0.4, 1, 0.65)$

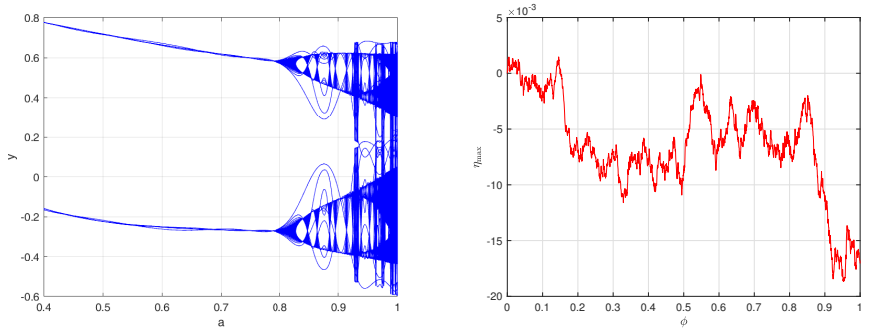

(g) $(\phi_1, \phi_2, \phi_3) = (0.4, 1, 0.30)$ **(h)** $(\phi_1, \phi_2, \phi_3) = (0.4, 1, 0.30)$

Figure 9. Bifurcation and MLEs plots for DFNN model (3.4) via the system parametric representations (δ_1, δ_2) and changing the values of DFOs (ϕ_1, ϕ_2, ϕ_3).

4. The $0-1$ test and complexity analysis for the proposed model

In this part, we examine the variety of chaotic behaviors in order to evaluate the exciting features of chaotic mechanisms, where the more extensive the intricacy is the more chaotic the structure becomes. This suggested DFNN model's (3.1) challenges are currently assessed using the approximate entropy (ApEn) examination and the $\mathbb{C}_0$ complexity technique. In addition, the $0-1$ approach will be used for verifying the occurrence of unpredictability in the DFNN framework (3.1).

4.1. The $0-1$ *test*

In this subsection, our goal is to apply the $0-1$ evaluation, a position developed by Gottwald and Melbourne [49] to distinguish within chaos and consistently practices complex mechanisms. We focus on the pattern of statistics as feedback, and when the framework's structure is chaotic, the resulting value is expected to be approximately one; alternatively, the outcome will be near zero. In addition, we represent the procedure in this manner: To begin, we determine the transformation factors outlined below employing the time analysis $(\mathbf{y}(\mathbf{r}))_{\mathbf{r}=1,...,\mathbf{N}}$:

$$\mathbf{p}_\psi(\jmath) = \sum_{\mathbf{r}=1}^{\jmath} \mathbf{y}(\mathbf{r})\cos(i\psi), \quad \mathbf{q}_\psi(\jmath) = \sum_{\mathbf{r}=1}^{\jmath} \mathbf{y}(\mathbf{r})\sin(i\psi), \quad \jmath = 1, 2, ..., \mathbf{N}. \tag{4.1}$$

The $(\mathbf{p}_\psi - \mathbf{q}_\psi)$ plot is applied to determine the extent to which the suggested DFNN structure exhibits chaotic practices. If the path vectors of $\mathbf{p}_\psi$ and $\mathbf{q}_\psi$ are restricted, the simulation's structure is periodic; whenever it shows Brownian-like performance, the framework's interactions are chaotic. In addition, we present the mean square displaced formulation as follows:

$$\Theta_\psi(\jmath) = \frac{1}{\mathbf{N}} \sum_{\mathbf{r}=1}^{\mathbf{N}} \left\{ \left(\mathbf{p}_\psi(\mathbf{r}+\jmath) - \mathbf{p}_\psi(\mathbf{r})\right)^2 + \left(\mathbf{q}_\psi(\mathbf{r}+\jmath) - \mathbf{q}_\psi(\mathbf{r})\right)^2 \right\}, \quad \mathbf{N} \geq 10\jmath. \tag{4.2}$$

Furthermore, we indicate asynchronous improvement as follows:

$$\mathcal{K}_\psi = \lim_{\jmath \mapsto \infty} \frac{\log \Theta_\psi}{\log \jmath}. \tag{4.3}$$

In the context of the provided commensurate DFNN system (3.1), the development rate "$\mathcal{K} = median(\mathcal{K}_\psi)$" permits to us differentiate between non-chaotic and erratic movement. When $\mathcal{K}$ corresponds to 0, the framework remains non-chaotic, while when $\mathcal{K}$ is adjacent to 1, the simulation is chaotic.

Figure 10 depicts the asynchronous rate of advancement $\mathcal{K}$ of the commensurate DFNN system (3.1) for $\phi \in [0.4, 1]$ where $\delta_1 = -8$ and $\delta_2 = 2.1$, respectively. Everyone recognizes that while the parameter δ_1 reduces, the development rate $\mathcal{K}$ reaches one, demonstrating that the commensurate DFNN model (3.1) exhibits erratic effects, which certainly demonstrates the earlier findings of bifurcations and their respective positions $\eta_{\max}$ presented in Figure 5. The outcomes of the **pq** diagrams involving varied incommensurate information and parameters are illustrated in Figure 11, respectively, confirming the presence of chaos within the incommensurate DFNN system (3.5). Figure 12(a-c) exhibits clearly confined pathways, indicating the fact that the mechanism is oscillatory. Figures 10

and 11, on the other hand, demonstrate Brownian-like pathways, confirming the presence of chaotic behaviors in the incommensurate DFNN system (3.5).

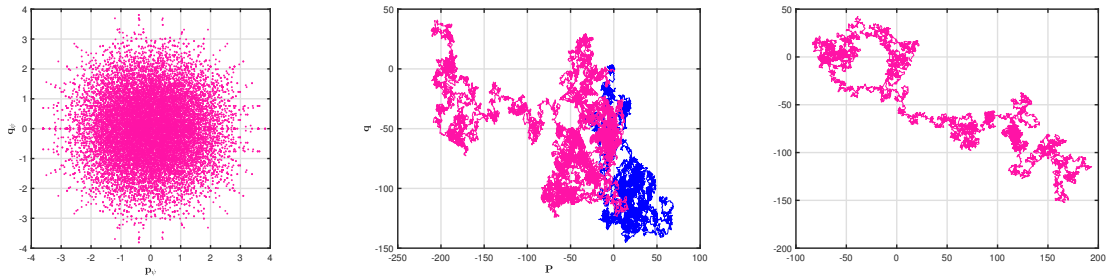

(a) $\phi = 0.96$ **(b)** $\phi = 0.67$ **(c)** $\phi = 0.46$

Figure 10. $\mathbf{P}_\psi - \mathbf{q}_\psi$ plots of the DFNN model (3.1) for parametric values (δ_1, δ_2) and varied DFO $\phi(0, 1]$.

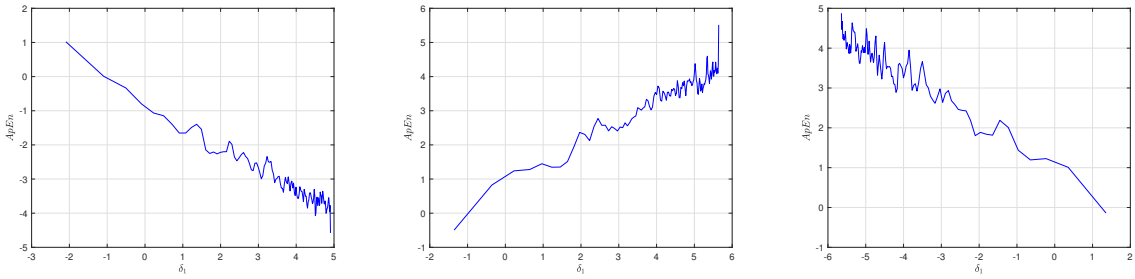

(a) **(b)** **(c)**

Figure 11. The ApEn plots of the DFNN model (3.1) and (3.5) via the parametric values (δ_1, δ_2) and DFO $\phi = 0.95$ and $(\phi_1, \phi_2, \phi_3) = (0.67, 1, 0.89)$.

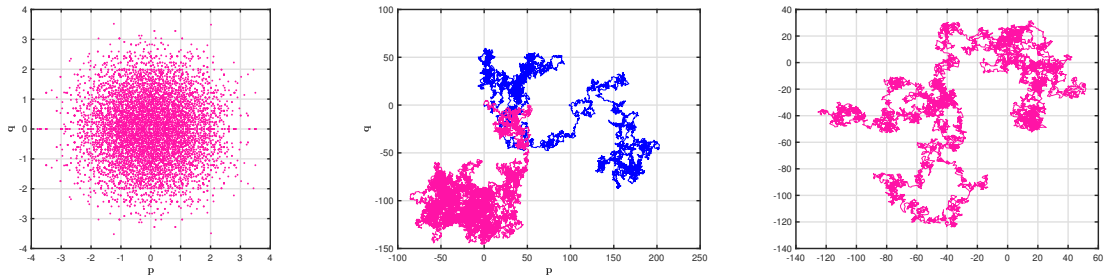

(a) $(\phi_1, \phi_2, \phi_3) = (0.65, 0.1, 0.1)$ **(b)** $(\phi_1, \phi_2, \phi_3) = (0.55, 0.9, 0.1)$ **(c)** $(\phi_1, \phi_2, \phi_3) = (1, 1, 0.45)$

Figure 12. $\mathbf{P}_\psi - \mathbf{q}_\psi$ illustrations of the DFNN model (3.5) for parametric values (δ_1, δ_2) and varying DFO (ϕ_1, ϕ_2, ϕ_3).

4.2. The ApEn of the proposed model

Currently, we employ the approximate entropy (ApEn) technique [50] for describing the intricate structure of the recurrent NN system (2.2). The ApEn is an indicator of the intricate nature of time-

based series-generated mechanisms. It should be noted that data sets containing greater ApEn numbers are more multifaceted. To compute ApEn, we identify the initial $\mathbf{n} - \mathbf{r} + 1$ transmissible forms below:

$$\mathbf{Q}(i) = [\mathbf{y}(i), ..., \mathbf{y}(i + \mathbf{r} - 1)], \quad \forall\, i \in [i + \mathbf{r} - 1], \tag{4.4}$$

where $\mathbf{y}(1), \mathbf{y}(2), ..., \mathbf{y}(\mathbf{n})$ is an assortment of separated points. Furthermore, we describe the components by using the formula $\mathbb{C}_i^{\mathbf{r}}(\mathbf{m}) = \mathcal{K}/(\mathbf{n} - \mathbf{r} + 1)$, where $\mathcal{K}$ is the dimension of $\mathbf{Q}(i)$ with $d(\mathbf{Q}(i), \mathbf{Q}(\mathbb{k})) \leq \mathbf{m}$. It should be noted that the ApEn is affected by two essential factors: the corresponding appreciation $\mathbf{m}$ as well as the embedded measurements $\mathbf{r}$. In this case, we put $\mathbf{r} = 2$ and $\mathbf{m} = 0.3\sqrt{var(\mathbf{Q})}$, where $\sqrt{var(\mathbf{Q})}$ is the positive square root of the variance of the data point $\mathbf{Q}$. In conceptual terms, the ApEn can be determined as:

$$ApEn = \phi^{\mathbf{r}}(\mathbf{m}) - \phi^{\mathbf{r}+1}(\ell), \tag{4.5}$$

where

$$\phi^{\mathbf{r}}(\mathbf{m}) = \frac{1}{\mathbf{n} - \mathbf{r} - 1} \sum_{i=0}^{\mathbf{n}-\mathbf{r}+1} \log \mathbb{C}_i^{\mathbf{r}}(\mathbf{m}). \tag{4.6}$$

Choosing the system's specifications $\delta_1 = -8$ and $\delta_2 = 2.12$ and ICs $(\mathbf{u}_1(0), \mathbf{u}_2(0), \mathbf{u}_3(0)) = (0.01, -0.01, 0.01)$, Figures 11 show the ApEn leads to commensurate DFNN system (3.1) as well as the incommensurate DFNN system (3.5). It becomes apparent that, in order to obtain greater ApEn, the period sequence must be more complex. As a consequence, these insights are consistent with whatever MLE outcomes have previously been demonstrated, validating the reality of chaos in the suggested fractional mechanism.

4.3. The $\mathbb{C}_0$ complexity of the suggested system

In what follows, we calculate the computational difficulty of the proposed recurrent NN system using the $\mathbb{C}_0$ complexity procedure employing the inverse Fourier transform. The technique is described in detail below [51].

The procedure for the computation of the $\mathbb{C}_0$ complexity during an order of $\phi(0), ..., \phi(\Theta - 1)$ is as outlined below:

Step 1: Calculate the Fourier transform of the term $\mathbf{u}_1(\mathbf{r})$ as:

$$\mathbf{Q_N}(\mathbf{t}) = \frac{1}{\mathbf{N}} \sum_{\Im=0}^{\mathbf{N}-1} \mathbf{u}_1(\Im) \exp\Big(- 2\pi i(\frac{j\mathbb{k}}{\mathbf{n}})\Big), \quad \Im = 0, 1, ..., \mathbf{N} - 1. \tag{4.7}$$

Step 2: The mean square is calculated as follows:

$$\mathbf{W_N} = \frac{1}{\mathbf{N}} \sum_{\Im=0}^{\mathbf{N}-1} |\mathbf{Q_N}(\Im)|^2, \tag{4.8}$$

where

$$\tilde{\mathbf{Q}}_{\mathbf{N}}(\Im) = \begin{cases} \mathbf{Q_N}(\Im) & if \quad \|\mathbf{Q_N}(\Im)\|^2 > \mathbf{mW_N}, \\ 0 & if \quad \|\mathbf{Q_N}(\Im)\|^2 \leq \mathbf{mW_N}. \end{cases} \tag{4.9}$$

Step 3: The inverse Fourier transform is calculated by employing the subsequent procedure:

$$\zeta(\mathbf{t}) = \frac{1}{\mathbf{N}} \sum_{\Im=0}^{\mathbf{N}-1} \tilde{\mathbf{Q}}_{\mathbf{N}}(\Im) \exp\Big(- 2\pi i(\frac{j\mathbb{k}}{\mathbf{n}})\Big), \quad \Im = 0, 1, ..., \mathbf{N} - 1. \tag{4.10}$$

Step 4: The procedure that follows is used to calculate $\mathbb{C}_0$'s degree of complexity:

$$\mathbb{C}_0 = \frac{1}{\sum\limits_{i=0}^{\mathbf{N}} \|\mathbf{u}_1(i)\|^2} \sum_{i=0}^{\mathbf{N}} \|\zeta(i) - \mathbf{u}_1(i)\|. \tag{4.11}$$

Figure 13 depicts the $\mathbb{C}_0$ complexity of the commensurate DFNN system (3.1) as well as demonstrating the outcomes of figuring out the $\mathbb{C}_0$ issues of the incommensurate DFNN model (3.5). We achieve these outcomes by modifying the structure's settings $(\delta_1, \delta_2) = (-70, 29)$ with ICs $(\mathbf{y}_1(0), \mathbf{y}_2(0), \mathbf{y}_3(0)) = (0, .01, -0.01, 0.01)$. As shown in Figure 13, the $\mathbb{C}_0$ measures of the commensurate system (3.1) improve just like the value of δ_2 declines. Additionally, when $(\phi_1, \phi_2, \phi_3) = (0.1, 0.9, 0.5)$, the incommensurate system (3.5) expresses less complexity as δ_2 rises and approaches 29.9, which is consistent regarding the splitting and the ApEn results. Moreover, the more substantial difficulties of the incommensurate framework (3.5) are visible in the range in which the setting δ_2 boosts (see Figure 13). As a result, we can conclude that the $\mathbb{C}_0$ complexity analysis is an effective way of efficiently assessing intricacy.

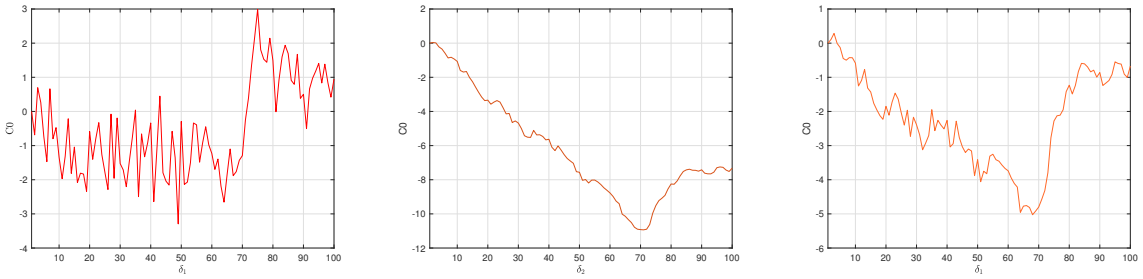

(a) **(b)** **(c)**

Figure 13. The $\mathbb{C}_0$ plots of the DFNN model (3.1) and (3.5) via the parametric values (δ_1, δ_2) and DFO $\phi = 0.95$ and $(\phi_1, \phi_2, \phi_3) = (0.67, 1, 0.89)$.

5. Controlling mechanism for the DFNN system

In this section, we provide a consolidation regulator for the suggested DFNN's chaotic pathways. The ultimate objective of the consolidation influence challenge is to create an effective responsive control that causes the entire system to diminish asynchronously to zero. To accomplish the above, we initially reminisce about the Lemma 2.3.

The regulated DFNN structure has now been provided by:

$$\begin{cases} {}^{c}\Delta_{\mathbf{b}}^{\phi}\mathbf{u}_1(\ell) = -\mathbf{u}_1(\ell - 1 + \phi) + \tanh\left(\mathbf{u}_2(\ell - 1 + \phi)\right) + \mathbf{v}_{\mathbf{u}_1}(\ell - 1 + \phi), \\ {}^{c}\Delta_{\mathbf{b}}^{\phi}\mathbf{u}_2(\ell) = -\mathbf{u}_2(\ell - 1 + \phi) + \tanh\left(\mathbf{u}_3(\ell - 1 + \phi)\right) + \mathbf{v}_{\mathbf{u}_2}(\ell - 1 + \phi), \\ {}^{c}\Delta_{\mathbf{b}}^{\phi}\mathbf{u}_3(\mathbf{t}) = -\mathbf{u}_3(\ell - 1 + \phi) + \delta_1 \tanh\left(\mathbf{u}_1(\ell - 1 + \phi)\right) + \delta_2 \tanh\left(\mathbf{u}_2(\ell - 1 + \phi)\right) \\ \qquad\qquad +\mathbf{v}_{\mathbf{u}_3}(\ell - 1 + \phi), \end{cases} \tag{5.1}$$

where $\mathbf{v}_{\mathbf{u}_1}(\ell)$, $\mathbf{v}_{\mathbf{u}_2}(\ell)$ and $\mathbf{v}_{\mathbf{u}_3}(\ell)$ are adaptation elements. The proposed regulation principle is illustrated by the hypothesis below:

Theorem 5.1. *The DFNN system* (3.1) *is kept stable by the governing law shown below:*

$$\begin{cases} \mathbf{v}_{\mathbf{u}_1}(\ell) = -\mathbf{u}_1(\ell) + \tanh\left(\mathbf{u}_2(\ell)\right), \\ \mathbf{v}_{\mathbf{u}_2}(\ell) = -\mathbf{u}_2(\ell) + \tanh\left(\mathbf{u}_3(\ell)\right), \\ \mathbf{v}_{\mathbf{u}_3}(\ell) = -\mathbf{u}_3(\ell) + \delta_1 \tanh\left(\mathbf{u}_1(\ell)\right) + \delta_2 \tanh\left(\mathbf{u}_2(\ell)\right). \end{cases} \tag{5.2}$$

Proof. By replacing (5.1) with (5.2), we obtain the subsequent framework:

$$\begin{cases} {}^{c}\Delta_{\mathbf{b}}^{\phi}\mathbf{u}_1(\ell) = -\mathbf{u}_1(\ell - 1 + \phi), \\ {}^{c}\Delta_{\mathbf{b}}^{\phi}\mathbf{u}_2(\ell) = -\mathbf{u}_2(\ell - 1 + \phi), \\ {}^{c}\Delta_{\mathbf{b}}^{\phi}\mathbf{u}_3(\mathbf{t}) = -\mathbf{u}_3(\ell - 1 + \phi). \end{cases} \tag{5.3}$$

Above expression can be written in the following form

$${}^{c}\Delta_{\mathbf{b}}^{\phi}(\mathbf{u}_1(\ell), \mathbf{u}_2(\ell), \mathbf{u}_3(\ell))^{\mathbf{T}} = Q(\mathbf{u}_1(\ell), \mathbf{u}_2(\ell), \mathbf{u}_3(\ell))^{\mathbf{T}}, \tag{5.4}$$

where

$$Q = \begin{pmatrix} -1 & 0 & 0 \\ 0 & -1 & 0 \\ 0 & 0 & -1 \end{pmatrix}. \tag{5.5}$$

Since $\varphi_1 = \varphi_2 = \varphi_3 = 1$ indicate the eigenvalues of Q, it is obvious that the eigenvalues $\varphi_{\mathbb{k}}$. $\mathbb{k} = 1, 2, 3$ meets the requirements of Lemma 2.3, proving that the regulated technique's (5.3) zero neutral state is asynchronously robust, and thus all phases of the regulated framework (5.3) are systematically controlled. □

The outcomes of Theorem 5.1 are displayed in Figure 14(a-c) and 15(a-c) for $\delta_1 = -8$ and $\delta_2 = 30.1$ with ICs $(0.01, -0.01, 0.01)$. Evidently, the regulated mechanism's tends to zero, as well as the chaotic aspect of the framework, which is removed.

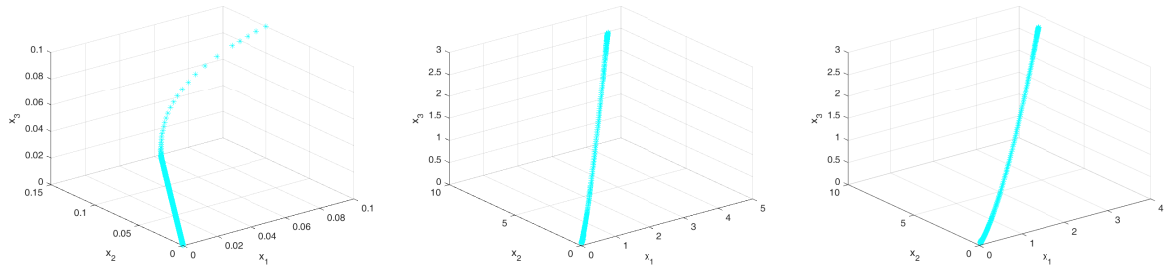

(a) $\phi = 0.97$ **(b)** $\phi = 0.77$ **(c)** $\phi = 0.54$

Figure 14. Chaos controlling of DFNN (5.3) with model parameters and various DFOs.

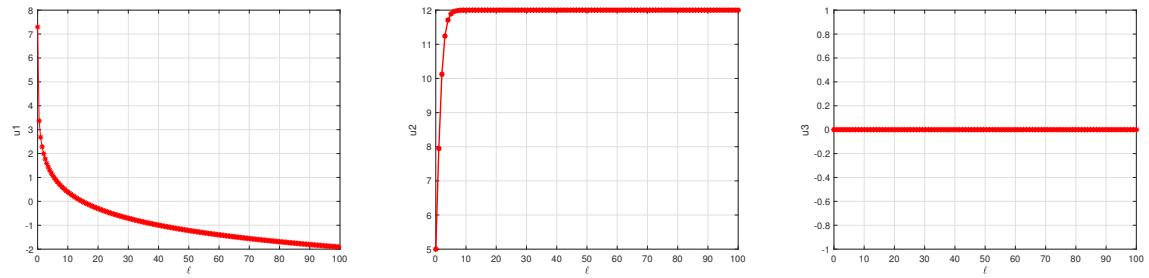

(a) $\phi = 0.67$ **(b)** $\phi = 0.67$ **(c)** $\phi = 0.67$

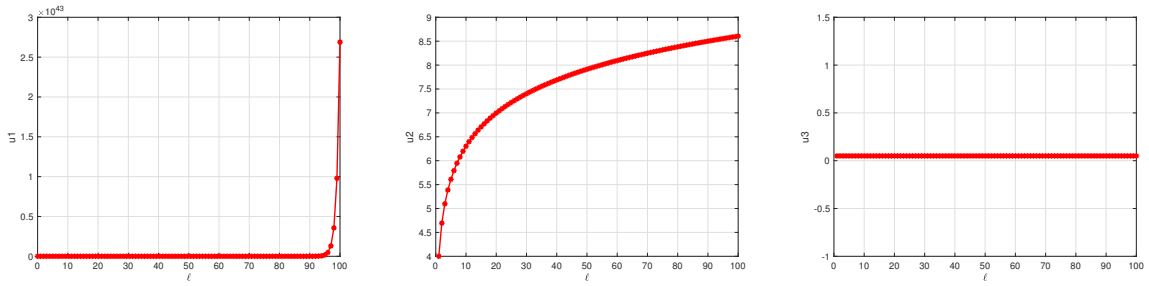

(d) $\phi = 0.79$ **(e)** $\phi = 0.79$ **(f)** $\phi = 0.79$

Figure 15. The stabilized illustrations of regulated DFNN system (5.3) for parametric variations (δ_1, δ_2) and ICs $(0.01, -0.01, 0.01)$.

5.1. Synchronization of the proposed system

The following portion introduces a dynamic operator for synchronizing the proposed DFNN framework (2.4) using undamped oscillations. The goal of synchrony is to compel any deviation within the slave and master mechanisms to come closer to zero.

Assume that the commensurate fractional system (2.4) is the governing framework:

$$\begin{cases} {}^{c}\Delta_{\mathbf{b}}^{\phi}\mathbf{u}_{1\mathbf{r}}(\ell) = -\mathbf{u}_{1\mathbf{r}}(\ell-1+\phi) + \tanh\left(\mathbf{u}_{2\mathbf{r}}(\ell-1+\phi)\right) + \mathbf{v}_{\mathbf{u}_{1\mathbf{r}}}(\ell-1+\phi), \\ {}^{c}\Delta_{\mathbf{b}}^{\phi}\mathbf{u}_{2\mathbf{r}}(\ell) = -\mathbf{u}_{2\mathbf{r}}(\ell-1+\phi) + \tanh\left(\mathbf{u}_{3\mathbf{r}}(\ell-1+\phi)\right) + \mathbf{v}_{\mathbf{u}_{2\mathbf{r}}}(\ell-1+\phi), \\ {}^{c}\Delta_{\mathbf{b}}^{\phi}\mathbf{u}_{3\mathbf{r}}(\ell) = -\mathbf{u}_{3\mathbf{r}}(\ell-1+\phi) + \delta_1 \tanh\left(\mathbf{u}_{1\mathbf{r}}(\ell-1+\phi)\right) + \delta_2 \tanh\left(\mathbf{u}_{2\mathbf{r}}(\ell-1+\phi)\right) \\ \qquad\qquad +\mathbf{v}_{\mathbf{u}_{3\mathbf{r}}}(\ell-1+\phi). \end{cases} \tag{5.6}$$

Introduce the slave system as:

$$\begin{cases} {}^{c}\Delta_{\mathbf{b}}^{\phi}\mathbf{u}_{1\hbar}(\ell) = -\mathbf{u}_{1\hbar}(\ell-1+\phi) + \tanh\left(\mathbf{u}_{2\hbar}(\ell-1+\phi)\right) + C_1(\ell-1+\phi), \\ {}^{c}\Delta_{\mathbf{b}}^{\phi}\mathbf{u}_{2\hbar}(\ell) = -\mathbf{u}_{2\hbar}(\ell-1+\phi) + \tanh\left(\mathbf{u}_{3\hbar}(\ell-1+\phi)\right) + C_2(\ell-1+\phi), \\ {}^{c}\Delta_{\mathbf{b}}^{\phi}\mathbf{u}_{3\hbar}(\ell) = -\mathbf{u}_{3\hbar}(\ell-1+\phi) + \delta_1 \tanh\left(\mathbf{u}_{1\hbar}(\ell-1+\phi)\right) + \delta_2 \tanh\left(\mathbf{u}_{2\hbar}(\ell-1+\phi)\right) \\ \qquad\qquad +C_3(\ell-1+\phi), \end{cases} \tag{5.7}$$

where the synchronization regulators perform C_1, C_2 and C_3, respectively. The synchronization

oversight for $\ell \in \mathbb{N}_{\mathbf{b}-1+\phi}$ is described below:

$$\begin{cases} \epsilon_1(\ell) = \mathbf{u}_{1\hbar}(\ell) - \mathbf{u}_{1\mathbf{r}}(\ell), \\ \epsilon_2(\ell) = \mathbf{u}_{2\hbar}(\ell) - \mathbf{u}_{2\mathbf{r}}(\ell), \\ \epsilon_3(\ell) = \mathbf{u}_{3\hbar}(\ell) - \mathbf{u}_{3\mathbf{r}}(\ell). \end{cases} \tag{5.8}$$

Considering that systems (5.6) and (5.7) are considered to be synchronized if $\lim_{\ell \mapsto \infty} |\epsilon_{\Bbbk}(\ell)| = 0, \ for \, \Bbbk = 1, 2, 3$. The upcoming result clarifies the proposed regulatory law for achieving mechanism synchronization.

Theorem 5.2. *Consider the system*

$$\begin{cases} C_1(\ell - 1 + \phi) = -(\mathbf{u}_{1\hbar}(\ell - 1 + \phi) - \mathbf{u}_{1\mathbf{r}}(\ell - 1 + \phi)) + (\tanh(\mathbf{u}_{2\hbar}(\ell - 1 + \phi)) \\ \qquad\qquad - \tanh(\mathbf{u}_{2\mathbf{r}}(\ell - 1 + \phi))) - \mathfrak{I}_1\epsilon_1(\ell), \\ C_2(\ell - 1 + \phi) = -(\mathbf{u}_{2\hbar}(\ell - 1 + \phi) - \mathbf{u}_{2\mathbf{r}}(\ell - 1 + \phi)) + (\tanh(\mathbf{u}_{3\hbar}(\ell - 1 + \phi)) \\ \qquad\qquad - \tanh(\mathbf{u}_{3\mathbf{r}}(\ell - 1 + \phi))) - \mathfrak{I}_2\epsilon_2(\ell), \\ C_3(\ell - 1 + \phi) = -(\mathbf{u}_{3\hbar}(\ell - 1 + \phi) - \mathbf{u}_{3\mathbf{r}}(\ell - 1 + \phi)) + \delta_1(\tanh(\mathbf{u}_{1\hbar}(\ell - 1 + \phi)) \\ \qquad\qquad - \tanh(\mathbf{u}_{1\mathbf{r}}(\ell - 1 + \phi))) + \delta_2(\tanh(\mathbf{u}_{2\hbar}(\ell - 1 + \phi)) \\ \qquad\qquad - \tanh(\mathbf{u}_{2\mathbf{r}}(\ell - 1 + \phi))) - \mathfrak{I}_3\epsilon_3(\ell), \end{cases} \tag{5.9}$$

where $\mathfrak{I}_{\Bbbk} \in (-1, 2^{\mathbf{b}} - 1)$, '$\Bbbk = 1, ..., 3$ *and* $0 < \mathfrak{I}_3 - d_2 < 2^{\mathbf{b}}$. *Then the systems defined in* (5.6) *and* (5.7) *are synchronized.*

Proof. By means of (2.5) and using the error approach stated in (5.8), we have

$$\begin{cases} {}^{c}\Delta_{\mathbf{b}}^{\phi}\epsilon_1(\ell) = -\mathbf{u}_{1\hbar}(\ell - 1 + \phi) + \tanh(\mathbf{u}_{2\hbar}(\ell - 1 + \phi)) + C_1(\ell - 1 + \phi) + \mathbf{u}_{1\mathbf{r}}(\ell - 1 + \phi) \\ \qquad\qquad - \tanh(\mathbf{u}_{2\mathbf{r}}(\ell - 1 + \phi)), \\ {}^{c}\Delta_{\mathbf{b}}^{\phi}\epsilon_2(\ell) = -\mathbf{u}_{2\hbar}(\ell - 1 + \phi) + \tanh(\mathbf{u}_{3\hbar}(\ell - 1 + \phi)) + C_2(\ell - 1 + \phi) + \mathbf{u}_{2\mathbf{r}}(\ell - 1 + \phi) \\ \qquad\qquad - \tanh(\mathbf{u}_{3\mathbf{r}}(\ell - 1 + \phi)), \\ {}^{c}\Delta_{\mathbf{b}}^{\phi}\epsilon_3(\mathbf{t}) = -\mathbf{u}_{3\hbar}(\ell - 1 + \phi) + \delta_1 \tanh(\mathbf{u}_{1\hbar}(\ell - 1 + \phi)) + \delta_2 \tanh(\mathbf{u}_{2\hbar}(\ell - 1 + \phi)) \\ \qquad\qquad + C_3(\ell - 1 + \phi) + \mathbf{u}_{3\hbar}(\ell - 1 + \phi) - \delta_1 \tanh(\mathbf{u}_{1\hbar}(\ell - 1 + \phi)) \\ \qquad\qquad - \delta_2 \tanh(\mathbf{u}_{2\hbar}(\ell - 1 + \phi)). \end{cases} \tag{5.10}$$

Plugging the control mechanism (5.9) into (5.10), we have

$${}^{c}\Delta_{\mathbf{b}}^{\nu}(\epsilon_1(\ell), \epsilon_2(\ell), \epsilon_3(\ell))^{\mathbf{T}} = \mathcal{Q}(\epsilon_1(\ell - 1 + \phi), \epsilon_2(\ell - 1 + \phi), \epsilon_3(\ell - 1 + \phi))^{\mathbf{T}},$$

where

$$\mathcal{Q} = \begin{pmatrix} -1 - \mathfrak{I}_1 & 0 & 0 \\ 0 & -1 - \mathfrak{I}_2 & 0 \\ 0 & 0 & -1 - \mathfrak{I}_3 \end{pmatrix}.$$

Since $\varphi_1 = \varphi_2 = \varphi_3 = -1 - \mathfrak{I}_{\Bbbk}$, $\Bbbk = 1, 2, 3$ indicate the eigenvalues of $\mathcal{Q}$, it is obvious that the eigenvalues $\varphi_{\Bbbk}$. $\Bbbk = 1, 2, 3$ meets the requirements of Lemma 2.3, the DFNN master framework (5.6) and slave model (5.7) are synchronously robust. □

Mathematical modeling employing MATLAB is used to validate this outcome. We select $(\delta_1, \delta_2) = (-8, 30.1)$, $(\Im_1, \Im_2, \Im_3) = (-0.1, -0.2, -0.3)$ and the initial values $(\epsilon_1(0), \epsilon_2(0), \epsilon_3(0)) = (-0.01.0.01, 0.01)$. The temporal progression of parts of the fractional oversight mechanism (5.8) dependent on manipulation rules (5.9) is depicted in Figure 16. It is unambiguous that the deviations are approaching zero, indicating that the synchronization addressed previously is productive.

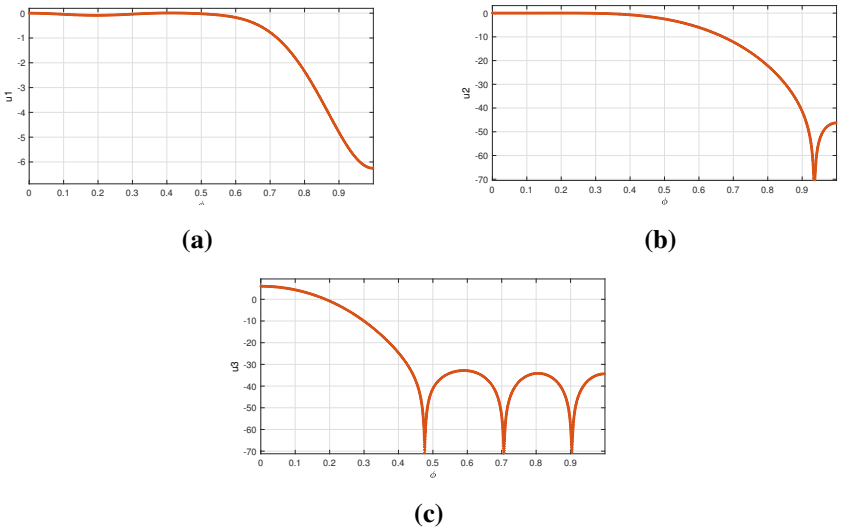

(a) **(b)**

(c)

Figure 16. Time dependent plots of the fractional error dynamics of (5.10).

6. Conclusions

In this paper, the undamped oscillations of the DFNN frameworks were studied using DFC. Obviously, FC has advantages over classical calculus, especially the limitless memory impact that contributes to greater abstraction of interactions. Meanwhile, we have supplied innovative features of the DFNN system that for investigating the potential of a discrete fractional three-node NN regarding commensurate or incommensurate orders to demonstrate distinctive dynamical patterns, such as equilibrium, bifurcations and fluctuations. We considered how these are influenced by the aforesaid procedure. The research indicated that the framework has convoluted and broad dynamic properties. Phase illustrations, generating bifurcation graphs, figuring out the MLE and performing the $0-1$ evaluation are all used to investigate the commensurate and incommensurate DFO scenarios. The ApEn procedure and the $\mathbb{C}_0$ examination have been employed to assess complexities, which demonstrated the framework's disorder. The findings reveal that the suggested framework yields chaotic patterns with a greater intricate extent and a wider spectrum of chaotic zones with varying DFO values. The states' convergence process is determined using the DFO discrete-time equilibrium concept. Finally, successful control laws were suggested that enable stabilizing and synchronizing the suggested model by compelling the states to converge toward zero asymptotically. Numerical simulations using MATLAB-21 were accomplished to validate our results. The linear growth procedure is used once more to determine oversight unification. Also, computational approaches are offered for verifying the results and demonstrating the viability of the suggested rules. Consequently, our results are comprehensive and more general in nature and capture all findings of [40] when fractional exponent

is assumed to be 1. The ultimate objective is to investigate the use of the fractional chaotic maps suggested in this article in digital encryption and signal processing. We will compare the outcomes of several encryption machine learning cases with prominent NNs, including the standard map.

Use of AI tools declaration

The authors declare they have not used Artificial Intelligence (AI) tools in the creation of this article.

Acknowledgements

The authors would like to acknowledge Deanship of Scientific Research, Taif University for funding this work.

Conflict of interest

The authors declare that they have no competing interests.

References

1. A. G. Radwan, On some generalized discrete logistic maps, *J. Adv. Res.*, **4** (2013), 163–171. https://doi.org/10.1016/j.jare.2012.05.003
2. H. Nejati, A. Beirami, Y. Massoud, A realizable modified tent map for true random number generation, *2008 51st Midwest Symposium on Circuits and Systems*, 2012. https://doi.org/10.1109/MWSCAS.2008.4616876
3. A. G. H. Rafash, E. M. H. Saeed, Al-S. M. Talib, Development of an enhanced scatter search algorithm using discrete chaotic Arnold's cat map, *East.-Eur. J. Enterp. Technol.*, **6** (2021), 15–20. https://doi.org/10.15587/1729-4061.2021.234915
4. M. Kaur, V. Kumar, Beta chaotic map based image encryption using genetic algorithm, *Internat. J. Bifur. Chaos*, **28** (2018), 1850132. https://doi.org/10.1142/S0218127418501328
5. N. Wang, D. Jiang, H. Xu, Dynamic characteristics analysis of a dual-rotor system with inter-shaft bearing, *Proc. Inst. Mech. Eng. Part G J. Aerospace Eng.*, **233** (2019), 1147–1158. https://doi.org/10.1177/0954410017748969
6. D. K. Arrowsmith, J. H. E. Cartwright, A. N. Lansbury, C. M. Place, The Bogdanov map: Bifurcation, mode locking and chaos in a dissipative system, *Internat. J. Bifur. Chaos*, **03** (1993), 803–842. https://doi.org/10.1142/S021812749300074X
7. A. Atangana, J. F. Gómez-Aguilar, Hyperchaotic behavior obtained via a nonlocal operator with exponential decay and Mittag-Leffler laws, *Chaos Solitons Fractals*, **102**(2017), 285–94. https://doi.org/10.1016/j.chaos.2017.03.022
8. A. Atangana, J. F. Gómez-Aguilar, Decolonisation of fractional calculus rules: Breaking commutativity and associativity to capture more natural phenomena, *Eur. Phys. J. Plus*, **133** (2018), 166. https://doi.org/10.1140/epjp/i2018-12021-3

9. A. Atangana, Application of fractional calculus to epidemiology, In: *Fractional dynamics*, 2015, 174–190. https://doi.org/10.1515/9783110472097-011
10. A. Atangana, J. F. Gómez-Aguilar, A new derivative with normal distribution kernel: Theory, methods and applications, *Phys. A*, **476** (2017), 1–14. https://doi.org/10.1016/j.physa.2017.02.016
11. J. F. Gómez-Aguilar, A. Atangana, New insight in fractional differentiation: power, exponential decay and Mittag-Leffler laws and applications, *Eur. Phys. J. Plus*, **132** (2017), 13. https://doi.org/10.1140/epjp/i2017-11293-3
12. W. Ou, C. Xu, Q. Cui, Z. Liu, Y. Pang, M. Farman, et al., Mathematical study on bifurcation dynamics and control mechanism of trineuron BAM neural networks including delay, *Math. Methods Appl. Sci.*, 2023. https://doi.org/10.1002/mma.9347
13. C. Xu, D. Mu, Y. Pan, C. Aouiti, L. Yao, Exploring bifurcation in a fractional-order predator-prey system with mixed delays, *J. Appl. Anal. Comput.*, **13** (2023), 1119–1136. https://doi.org/10.11948/20210313
14. C. Xu, Z. Liu, P. Li, J. Yan, L. Yao, Bifurcation mechanism for fractional-order three-triangle multi-delayed neural networks, *Neural Process. Lett.*, **55** (2023), 6125–6151. https://doi.org/10.1007/s11063-022-11130-y
15. W. Ahmad, R. El-Khazali, A. El-Wakil, Fractional order Wien-bridge oscillator, *Electron. Lett.*, **37** (2001), 1110–1112. https://doi.org/10.1049/el:20010756
16. Y. Wang, C. Li, Does the fractional Brusselator with efficient dimension less than 1 have a limit cycle?, *Phys. Lett. A*, **363** (2007), 414–419. https://doi.org/10.1016/j.physleta.2006.11.038
17. J. Cao, C. Ma, Z. Jiang, S. Liu, Nonlinear dynamic analysis of fractional order rub-impact rotor system, *Commun. Nonlinear Sci. Numer. Simul.*, **16** (2011), 1443–1463. https://doi.org/10.1016/j.cnsns.2010.07.005
18. H. A. El-Saka, E. Ahmed, M. I. Shehata, A. M. A El-Sayed, On stability, persistence and Hopf bifurcation in fractioanl order dynamical systems, *Nonlinear Dyn.*, **56** (2009), 121–126. https://doi.org/10.1007/s11071-008-9383-x
19. J. J. Hopfield, Neurons with graded response have collective computational properties like those of two-state neurons, *Proc. Natl. Acad. Sci. USA*, **81** (1984), 3088–3092. https://doi.org/10.1073/pnas.81.10.3088
20. L. P. Shayer, S. A. Campbell, Stability, bifurcation, and multistability in a system of two coupled neurons with multiple time delays, *SIAM J. Appl. Math*, **61** (2000), 673–700. https://doi.org/10.1137/S0036139998344015
21. J. Wei, M. Y. Li, Global existence of periodic solutions in a tri-neuron model with delays, *Phys. D*, **198** (2004), 106–119. https://doi.org/10.1016/j.physd.2004.08.023
22. J. Cao, M. Xiao, Stability and Hopf bifurcation in a simplified BAM neural network with two time delays, *IEEE Trans. Neural Networ.*, **18** (2007), 416–430. https://doi.org/10.1109/TNN.2006.886358
23. K. S. Cole, Electric conductance of biological systems, *Cold Spring Harb. Symp. Quant. Biol.*, 1993, 107–116.

24. T. J. Anastasio, The fractional-order dynamics of brainstem vestibule-oculumotor neurons, *Biol. Cybernet.*, **72** (1994), 69–79. https://doi.org/10.1007/bf00206239

25. F. M. Atici, P. W. Eloe, Discrete fractional calculus with the Nabla operator, *Electron. J. Qual. Theo. Differ. Equ.*, 2009, 1–12.

26. T. Abdeljawad, On Riemann and Caputo fractional differences, *Comput. Math. Appl.*, **62** (2011), 1602–1611. https://doi.org/10.1016/j.camwa.2011.03.036

27. T. Abdeljawad, D. Baleanu, F. Jarad, R. P. Agarwal, Fractional sums and differences with binomial coefficients, *Discrete Dyn. Nat. Soc.*, **2013** (2013), 104173. https://doi.org/10.1155/2013/104173

28. C. Goodrich, A. C. Peterson, *Discrete fractional calculus*, Springer Cham, 2015. https://doi.org/10.1007/978-3-319-25562-0

29. D. Baleanu, G. Wu, Y. Bai, F. Chen, Stability analysis of Caputo-like discrete fractional systems, *Commun. Nonlinear Sci. Numer. Simul.*, **48** (2017), 520–530. https://doi.org/10.1016/j.cnsns.2017.01.002

30. Y. M. Chu, T. Alzahrani, S. Rashid, W. Rashidah, S. ur Rehman, M. Alkhatib, An advanced approach for the electrical responses of discrete fractional-order biophysical neural network models and their dynamical responses, *Sci. Rep.*, **13** (2023), 18180. https://doi.org/10.1038/s41598-023-45227-8

31. G. C. Wu, D. Baleanu, Discrete chaos in fractional delayed logistic maps, *Nonlinear Dyn.*, **80** (2015), 1697–703. http://doi.org/10.1007/s11071-014-1250-3

32. T. Hu, Discrete chaos in fractional Hénon map, *Appl. Math.*, **5** (2014), 2243–2248. http://doi.org/10.4236/am.2014.515218

33. M. Edelman, On stability of fixed points and chaos in fractional systems, *Chaos*, **28** (2018), 023112. https://doi.org/10.1063/1.5016437

34. A. L. Fradkov, R. J. Evans, Control of chaos: Methods and applications in engineering, *Annu. Rev. Control*, **29** (2005), 33–56. https://doi.org/10.1016/j.arcontrol.2005.01.001

35. A. L. Fradkov, R. J. Evans, B. R. Andrievsky, Control of chaos: Methods and applications in mechanics, *Phil. Trans. R. Soc. A.*, **364** (2006), 2279–2307. http://doi.org/10.1098/rsta.2006.1826

36. G. Wu, D. Baleanu, H. Xie, F. Chen, Chaos synchronization of fractional chaotic maps based on the stability condition, *Phys. A*, **460** (2016), 374–283. https://doi.org/10.1016/j.physa.2016.05.045

37. Y. Liu, Chaotic synchronization between linearly coupled discrete fractional Hénon maps, *Indian J. Phys.*, **90** (2016), 313–317. https://doi.org/10.1007/s12648-015-0742-4

38. O. Megherbi, H. Hamiche, S. Djennoune, M. Bettayeb, A new contribution for the impulsive synchronization of fractional-order discrete-time chaotic systems, *Nonlinear Dyn.*, **90** (2017), 1519–1533. https://doi.org/10.1007/s11071-017-3743-3

39. H. L. Gray, N. F. Zhang, On a new definition of the fractional difference, *Math. Comput.*, **50** (1988), 513–529. https://doi.org/10.1090/S0025-5718-1988-0929549-2

40. A. C. Ruiz, D. H. Owens, S. Townley, Existence, learning, and replication of periodic motions in recurrent neural networks, *IEEE Trans. Neural Netw*, **9** (1998), 651–661.

41. S. Townley, A. Ilchmann, M. G. Weiss, W. Mcclements, A. C. Ruiz, D. H. Owens, et al., Existence and learning of oscillations in recurrent neural networks, *IEEE Trans. Neural NetwOR.*, **11** (2000), 205–214. https://doi.org/10.1109/72.822523

42. M. Xiao, W. X. Zheng, G. P. Jiang, J. D. Cao, Undamped oscillations generated by Hopf bifurcations in fractional-order recurrent neural networks with Caputo derivative, *IEEE Trans. Neura. Net. Lear. Syst.*, **26** (2015), 3201–3214. https://doi.org/10.1109/TNNLS.2015.2425734

43. J. Cermak, I. Gyori, L. Nechvatal, On explicit stability conditions for a linear fractional difference system, *Fract. Cal. Appl. Anal.*, **18** (2015), 651–672. https://doi.org/10.1515/fca-2015-0040

44. M. S. Tavazoei, M. Haeri, M. Attari, S. Bolouki,M. Siami, More details on analysis of fractional-order Van der Pol oscillator, *J. Vib. Control*, **15** (2009), 803–819. https://doi.org/10.1177/1077546308096101

45. F. R. Gantmakher, *The theory of matrices*, New York: Chelsea Publishing Company, 1959.

46. M. A. Qurashi, Q. U. A. Asif, Y. M. Chu, S. Rashid, S. K. Elagan, Complexity analysis and discrete fractional difference implementation of the Hindmarsh-Rose neuron system, *Results Phy.*, **51** (2023), 106627. https://doi.org/10.1016/j.rinp.2023.106627

47. M. A. Qurashi, S. Rashid, F. Jarad, E. Ali, R. H. Egami, Dynamic prediction modeling and equilibrium stability of a fractional discrete biophysical neuron model, *Results Phys.*, **48** (2023), 106405. https://doi.org/10.1016/j.rinp.2023.106405

48. M. S. Tavazoei, M. Haeri, N. Nazari, Analysis of undamped oscillations generated by marginally stable fractional order systems, *Signal Process.*, **88** (2008), 2971–2978. https://doi.org/10.1016/j.sigpro.2008.07.002

49. G. A. Gottwald, I. Melbourne, The 0–1 test for chaos: A review, In: *Chaos detection and predictability*, Heidelberg: Springer, **915** (2016), 221–247. https://doi.org/10.1007/978-3-662-48410-4_7

50. S. M. Pincus, Approximate entropy as a measure of system complexity, *Proc. Natl. Acad. Sci. USA*, **88** (1991), 2297–2301. https://doi.org/10.1073/pnas.88.6.2297

51. E. H. Shen, Z. J. Cai, F. J. Gu, Mathematical foundation of a new complexity measure, *Appl. Math. Mech.*, **26** (2005), 1188–1196. https://doi.org/10.1007/bf02507729

AIMS Press